Combustion dynamics of annular systems.

Guillaume Vignat, D. Durox, Thierry Schuller, Sébastien Candel

Combustion Dynamics of Annular Systems

G. Vignat[a], D. Durox[a], T. Schuller[b], and S. Candel[a]

[a]EM2C Laboratory, CNRS, CentraleSupélec, University Paris-Saclay, Gif-sur-Yvette cedex, France; [b]Institut de Mécanique des Fluides de Toulouse, IMFT, Université de Toulouse, CNRS, Toulouse, France

ABSTRACT

New results on the dynamics of annular combustors during ignition and combustion instabilities will be reviewed. Ignition dynamics is considered first by examining experiments carried out in a system comprising a plenum feeding premixed gaseous reactants through multiple swirling injectors and an annular combustor formed by two concentric transparent quartz walls allowing full optical access to the flame. The analysis focuses on the "light-round" process during which the flame spreads from one injector to the next eventually leading to established flames on each injector. The transparent lateral walls allow a full view of the flame propagation from a spark igniter located in the neighborhood of one injector. High speed imaging is used to examine flame displacement and deduce the ignition delay yielding a full light around of the annular combustor. Changes associated to operation with spray flames are then discussed. The second part of this article is concerned with combustion instabilities of annular systems coupled by azimuthal modes. This type of oscillation has received considerable attention in recent years because the underlying coupling is often observed in the advanced premixed combustion architectures used in modern gas turbines. Recent studies have allowed a detailed examination of the dynamics of annular devices comprising multiple swirling injectors. Experiments on annular systems and single sector configurations provide new insight on the coupling process between acoustics and unsteady combustion. Results for self-sustained combustion oscillations coupled by azimuthal modes are presented for operation with gaseous premixed reactants and with spray flames.

Introduction

A considerable amount of research in combustion deals with dynamical issues. These investigations were initially motivated by problems encountered during early developments of high performance devices and in particular those of liquid rocket and jet engines and more recently by difficulties in operating gas turbines featuring low NOx premixed combustor architectures. Pioneering work in the field of combustion instability was initiated in the early fifties by various groups and in particular by Luigi Crocco, a professor at Princeton, and his students and colleagues with among others William Sirignano, the central figure of the present colloquium that honors his sixty years of contributions to the advancement of science.

Much of the early work of this period emphasized the existence of time lags in combustion processes associated for example with the vaporization of propellant droplets and the

sensitivity of the corresponding delays to state variables (Crocco 1951, 1952; Crocco and Cheng 1953, 1956; Marble and Cox 1953; Tsien 1952). Many investigations were also concerned with the effect of the nozzle and the associated boundary condition (Crocco and Sirignano 1966; Zinn and Crocco 1968). Research by the Princeton group underlined the nonlinear features associated with the large amplitude perturbations arising under combustion instability, see for example Mitchell, Crocco, and Sirignano (1969); Sirignano and Crocco (1964). The effort on liquid rocket engine combustion instability was synthesized in a report (NASA SP194) edited by Harrje and Reardon (1972).

Investigation of liquid rocket instabilities has been continued by Sirignano and coworkers over the years, see for example Popov and Sirignano (2016); Popov, Sirignano, and Sideris (2015); Sirignano and Krieg (2016); Sirignano and Popov (2013), and a review of his early and more recent contributions dealing with this topic may be found in Sirignano (2015). With respect to these classical and modern studies recent investigations have emphasized detailed experimentations exploiting digital imaging, optical diagnostics and digital data processing in combination with numerical simulations. The processes involved in the combustion of cryogenic propellants have been investigated using single injector configurations operating at high pressure above the critical pressure of oxygen, see Juniper et al. (2000) and Candel et al. (2006) for a review. Experiments on the interaction between transverse acoustic modes in a system compring multiple injectors have provided insights on the flame dynamics under very high amplitude modulation, see for example Mery et al. (2013); Richecoeur et al. (2006). On the theoretical/numerical side much progress has been accomplished by making use of nonlinear tools to describe the flame dynamics or by exploring the possibilities of high performance computing and large eddy simulation, see for example Hakim et al. (2015a, 2015b); Schmitt et al. (2011). Large eddy simulations have also been used to explore liquid rocket instabilities in a realistic configuration comprising a large number of coaxial injectors by Urbano et al. (2016, 2017).

The current effort in the field of combustion instability is motivated by issues raised by gas turbine combustors (Poinsot 2017). Table 1 summarizes characteristics of high performance devices that influence their combustion dynamics. While rocket thrust chambers are cylindrical and terminated by a choked nozzle, combustors are annular in modern aero-engine and in most stationary gas turbine. The downstream boundary condition is formed by the turbine distributor. In most cases these devices feature an annular geometry and the combustion dynamics of such systems raises fundamental issues and in particular those associated with the coupling by azimuthal chamber modes. Operation under lean conditions and the relatively high energy density associated with the compact flame region promotes the development of such oscillations. The absence of perforated liners in partially premixed systems also reduces damping characteristics. In the annular geometry, one finds in addition to longitudinal instabilities, oscillations coupled by tangential modes that are less well damped. The problem is compounded by the fact that flames are likely to respond over a wide frequency range, and the modal density in the annular geometry can be quite high. If a resonant mode disappears because the combustion regime has been modified, or because the thermal or impedance conditions are changed, another acoustic mode may be initiated.

Many of these issues are considered in a book edited by Lieuwen and Yang (2005) while Huang and Yang (2009) provide an extensive review of multidimensional simulation efforts and low order dynamical modeling. In general predictions are based on measurements of the flame transfer function (FTF) which are combined with acoustic network

representations of the system. This linear analysis gives access to stability maps, resonant frequencies and growth rates (Dowling and Stow 2003; Durox et al. 2013; Sattelmayer and Polifke 2003; Schuller, Durox, Candel 2003). This approach has become reasonably mature that it can be successfully applied to industrial configurations, even at elevated pressure as indicated for example by Schuermans et al. (2010). The linear approach can be extended to deal with nonlinear features by making use of the describing function, a concept used for example by Dowling (1997) to represent the dynamics of a ducted flame. The flame describing function (FDF) representing the flame response in combination with an acoustic network or in combination with a Helmholtz solver yields growth rates and frequencies depending on the amplitude of oscillation. As shown by Noiray et al. (2008) and Boudy et al. (2011) this framework gives access to nonlinear phenomena like frequency shifting, mode switching triggering and hysteresis. The FDF has been applied more recently to instabilities of systems equipped with a swirling injector (Palies et al. 2011; Silva et al. 2013; Cosic, Moeck, and Paschereit 2014) and to annular systems (Ghirardo, Juniper, Moeck 2016; Laera et al. 2017; Yang, Laera, Morgans 2019). Large eddy simulations have been used to predict the dynamical processes in gas turbine combustors, either as input to low order models based on the FTF and FDF frameworks, or for direct simulation of unstable combustion systems. These subjects are reviewed by Gicquel, Staffelbach, and Poinsot (2012) and Poinsot (2017).

In most gas turbine combustors flames are stabilized by swirling injectors. This has led to detailed examination of the dynamics of swirling flames. In these systems the flame is anchored by imparting an azimuthal component to the flow usually by passing the air stream through a swirler or through a set of swirlers. The rotation induced by these devices generates a central recirculation zone (CRZ) and in many cases an outer recirculation zone (ORZ) which are filled with hot combustion products which continuously ignite the fresh reactants injected in the combustor.

The dynamics of swirling flames thus constitutes a basic topic that has received considerable attention in recent years (see Candel et al. (2014) for a recent review). Swirling flames were found to be subject to a variety of direct and indirect excitation mechanisms. Under the effect of acoustic forcing, the annular jet formed in the swirling flow fluctuates, and the vortex breakdown bubble is dynamically displaced. This results in deformations of the flame front and oscillations of the flame anchor point (Borghesi, Biagioli, Schuermans 2009; Gatti et al. 2019; Thumuluru and Lieuwen 2009). If the fuel is injected close to or inside the swirler, a situation which is typically found in practical systems, acoustic perturbations at the injector generate fluctuations in the mixture ratio. These are convected to the flame and cause heat release rate fluctuations by modifying the burning velocity (Lieuwen et al. 2001). Another indirect effect is related to the interaction of incident acoustic waves with the swirler. This process generates fluctuations in the azimuthal velocity that perturb the flame after a convective delay (Huang and Yang 2009; Komarek and Polifke 2010; Palies et al. 2010). The interference between perturbations propagating at acoustic and convective velocities leads to a specific frequency dependence of the flame response. Swirl flames are also receptive to transverse acoustic forcing and this may be relevant to azimuthal instabilities observed in annular combustors. Generally, the swirling flame response to transverse acoustic forcing depends on the orientation of the acoustic field (O'Connor, Acharya, Lieuwen 2015). If a pressure antinode is located at the flame, axial acoustics will be excited and these axial fluctuations dominate the flame

Table 1. General characteristics of high performance devices of importance for their combustion dynamics analysis.

System	Liquid rocket Engines	Aero-engines	Gas turbines
Power density	Very high $\simeq$ 50 GW m^{-3}	High $\simeq$ 1 GW m^{-3}	High, $\simeq$ 1 GW m^{-3}
Chamber pressure	Very high, $\simeq$ 10 MPa	High 3 to 5 MPa	High 1.7 to 3.5 MPa
Combustion mode	Non premixed	Partially premixed	Essentially premixed
Chamber geometry	Cylindrical	Annular	Often annular
Upstream boundary	Propellant domes	High pressure Compressor	High pressure Compressor
Dowstream boundary	Choked nozzle	Turbine distributor	Turbine distributor
Injection	Shear coaxial low swirl	Swirling injectors, Hollow cone or multipoint atomizers	Swirling injectors
State of fuel and oxidizer	Liquid-liquid or liquid-gas No diluent	Liquid fuel and air Nitrogen diluent in air stream	Gaseous fuel and air, Nitrogen diluent in air stream

response. For the case of a transverse velocity antinode, it is found that non-axisymmetric shear layer modes are excited which interact with the flame.

In practical cases the swirling flow is confined by lateral walls in a geometry which features in many cases an annular cross section and by transverse flows originating from lateral orifices. The presence of these side walls, transverse jets and neighboring injectors has a significant impact on the flow structure complicating the analysis (Fanaca et al. 2010; Han and Morgans 2018; Worth and Dawson 2019). Studies of a single injector placed in a sector or in an axisymmetric configuration provides useful information but only approximately represent the practical situation. This clearly underlines the necessity to work on fully annular configurations allowing azimuthal mode coupling.

A substantial amount of literature exists in the field of combustion instabilities but the majority of experimental investigations consider oscillations coupled by longitudinal modes in single injector configurations, see review articles Candel (2002); Culick (2001); Huang and Yang (2009); Poinsot (2017); Putnam (1971). The problem of azimuthal mode coupling in combustion instabilities is considered in recent theoretical investigations (Bauerheim et al., 2014a, 2014b; Evesque, Polifke, Pankiewitz 2003; Ghirardo and Juniper 2013; Ghirardo, Juniper, Moeck 2016; Noiray, Bothien, Schuermans 2011; Noiray and Schuermans 2013; Pankiewitz and Sattelmayer 2003; Schuermans, Bellucci, Paschereit 2003; Stow and Dowling 2001). A central issue is to account for the collective processes where neighboring flames interact and feed energy in the azimuthal modes.

Experimental investigations on well instrumented annular chambers are not common. Kopitz et al. (2005) used a network model to analyze the stability of an experimental annular combustor exhibiting two different instabilities depending on the operating conditions, a longitudinal mode and a first-order azimuthal mode. The flame response measured at stable conditions was extrapolated in flow rate and equivalence ratio to the unstable regime. Both modes could be identified in the model but only the instability of

coupled by a longitudinal mode was accurately captured. Moeck, Paul, and Paschereit (2010) explored azimuthal instabilities of an annular chamber equipped with 12 channels comprising electrically heated Rijke tubes. Also, the Rijke tubes sucked air from the surrounding atmosphere and there was no plenum or upstream manifold. Depending on the electrical power injected, two azimuthal modes were observed in the form of a standing wave or a slowly spinning oscillation. Staging in the heating tubes was tested to see if this could help stabilize the system. It was found that some modes could be attenuated, while others were strengthened. An acoustic model was used to predict the dynamical behavior of the annular chamber and test the influence of staging. Krebs et al. (2002) were the first authors reporting detailed experimental data for the acoustic pressure distribution in an instrumented industrial gas turbine featuring self-sustained combustion oscillations coupled to one of the azimuthal modes of the combustion chamber. Their analysis places particular emphasis on the role of the acoustic boundary conditions and flame response in the development of spinning and standing modes.

In this general context it appears logical to consider the dynamics of annular configurations comprising multiple injectors. This review is based on experimental data gathered in two model scale annular combustor facilities developed in recent years. They both feature a transparent combustion chamber to see the flames over all the injectors regularly distributed along the azimuthal direction. In both cases the objective was to gather knowledge on ignition and azimuthal instabilities in annular configurations. The first described by Worth & Dawson (2013b) was initially designed in Cambridge. Interesting aspects of the dynamics of this annular system are explored in a series of articles (Dawson and Worth 2014, 2015; Worth & Dawson, 2013a; Worth et al. 2017). Ignition dynamics is also investigated in the Cambridge annular combustor by (Machover and Mastorakos 2016, 2017).

This experimental device, shown in Figure 1, has a relatively small chamber diameter of 17 cm. The number of injectors connecting the plenum to the chamber backplane can be changed. Experiments were carried out with 12, 15 or 18 units allowing a change in the spacing to diameter ratio. Injectors are swirled but the swirl number is moderate and there is a central bluff-body which occupies 50% of the injector exhaust section. The fresh gases are then exhausted through a thin annular slit. Azimuthal instabilities are obtained by operating with a mixture of ethylene and air, and by making use of an interior chamber wall shorter than the outer wall (13 cm and 17 cm respectively). For an equivalence ratio above 0.85, a strong azimuthal instability is observed taking the form of a spinning or standing wave depending on the spacing between injectors. The instability is enhanced when the flames are close giving rise to strong interactions between adjacent reactive layers. For pressure oscillations with an amplitude of 200 Pa in the chamber, the fluctuation in heat release rate quoted in Worth & Dawson (2013a) is around 10%.

Another experimental setup MICCA developed independently in our laboratory (Bourgouin et al. 2013a, 2013b) provides additional information on instabilities coupled by azimuthal modes. The geometry has some features in common with that of Worth and Dawson (2013a) but there are differences. The MICCA test facility was designed to identify the physical mechanisms driving instabilities of annular combustors and provide experimental data for model validation. Dimensions of MICCA differ from those used in Worth and Dawson (2013a), a choice guided by considerations of flame receptivity to flow perturbations. By selecting a large diameter, resonant frequencies corresponding to

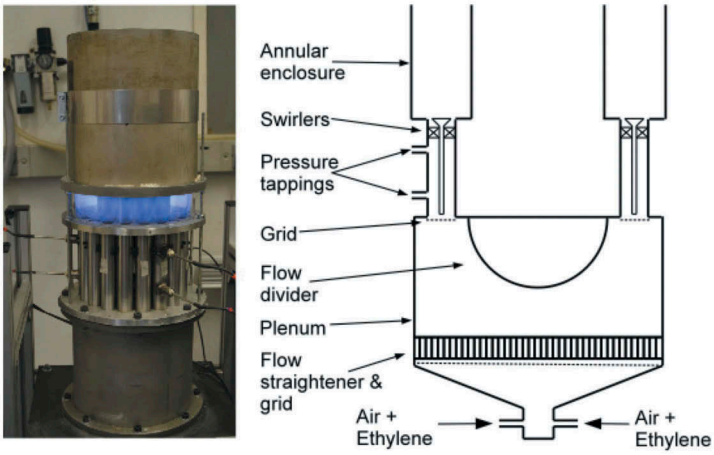

Figure 1. Left: view of the system under operation. The mean diameter of the ring is 170 mm. Injectors comprise a central bluff body. Right: Schematic diagram of the setup. Reproduced from Worth and Dawson (2013b).

azimuthal modes are reduced and can be brought inside the range where the flame transfer function has a finite gain. In particular, the mean diameter of the MICCA combustor of 35 cm is close to that of a helicopter gas turbine and is twice that of the Cambridge experiment. The annular chamber is equipped with 16 swirl injectors. The swirl number is sufficiently high to allow flame anchoring without requiring a central bluff-body. The flame dynamics is then closer to that found in practical devices where combustion is stabilized aerodynamically by swirl in the absence of a central obstacle. The chamber operates at atmospheric pressure and it is fully transparent to allow observations with a high speed camera. Waveguide microphones are used to record pressure signals at the combustor injection plane and inside the annular plenum. Depending on operating modes, the system exhibits longitudinal or azimuthal instabilities (Bourgouin et al. 2013a).

The MICCA facility has evolved into a number of different versions as illustrated in Figure 2. The initial configuration was equipped with injectors fed by premixed reactants featuring a cylindrical exhaust section (Bourgouin et al. 2013b). These injectors were later fitted with a conical cup and the corresponding configuration was designated as MICCA2 (Durox et al. 2016). Swirling units were then replaced by matrix injectors comprising a periodic arrangement of small channels producing a multiplicity of small laminar flames. This version (MICCA3) has allowed investigations of combustion instabilities coupled by azimuthal modes in the absence of complexities associated with turbulence and swirling flows (Bourgouin et al., 2015a, 2015b; Prieur et al., 2017a). It was modified more recently to allow liquid fuel injection in the form of a spray using hollow cone atomizers. This configuration designated as MICCA-Spray is used to test a variety of swirling injection units and in particular to document effects of swirl number and injector head loss (Prieur et al., 2017b; Prieur et al. 2018, 2019).

The present review essentially deals with fundamental items pertaining to ignition dynamics and combustion instabilities of annular systems. There is no intention to provide an exhaustive review but merely to give a synthesis of research carried out in relation with the MICCA annular combustor facility. The first item designated as the “light-round” essentially

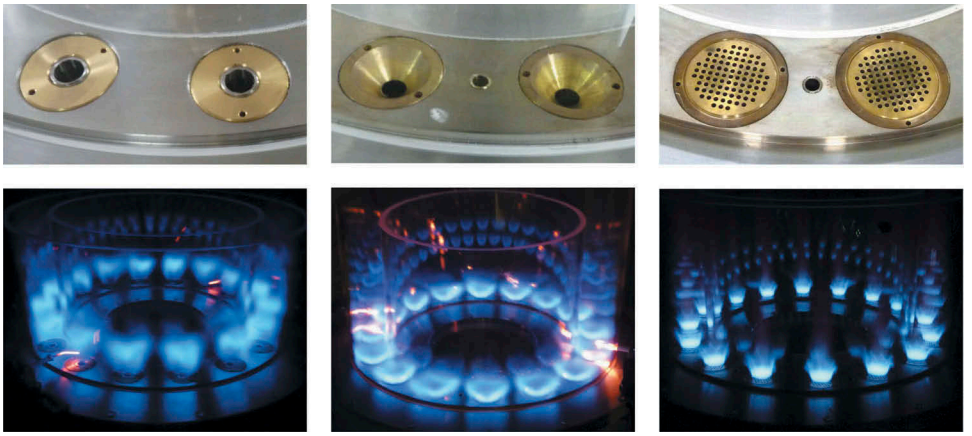

Figure 2. Injector geometry and induced flame shape in the annular setup. Left: MICCA, the injectors feature a swirler and a cylindrical exhaust channel. This configuration is used in the light-round investigation. Center: MICCA2, the injectors feature a swirler and a conical cup. This geometry is used in the thermo-acoustics instability investigations. Right: MICCA3 with matrix injectors used to examine thermo-acoustics instabilities in an environment which features low levels of random perturbations.

concerns the circumferential propagation of the flame from an initial kernel formed by a spark plug to the final stabilization of combustion in the system (Section 2). The second item is specifically concerned with oscillations coupled by modes that span the circumference of the annulus. An experimental methodology is first introduced that combines single sector investigations targeted at injector characterization and selection with testing in the annular configuration (Section 3). Instabilities of annular systems are then discussed (Section 4). The premixed case is considered first because much of the recent work on swirling flames has been carried out in relation with the design of advanced premixed combustion technologies with the objective of reducing NOx emissions from gas turbines. These systems have achieved low pollutant levels but their operation has been hindered by dynamical phenomena. This is so because premixed flames are more compact and more sensitive to external perturbations. Also damping in lean premixed systems is reduced because the perforated liners found in more standard designs are for the most part eliminated in modern premixed combustors. It is next interesting to examine situations where the fuel is injected as a liquid spray of droplets as in aero-jet gas turbine engines (Section 5). This will be accomplished by making use of the MICCA-Spray configuration fed by swirl spray atomizers.

Ignition dynamics in annular configurations

Ignition issues are extensively studied in the literature. Research has concerned a variety of topics such as conditions at the spark gap like minimum spark energy (Ballal and Lefebvre 1974; Lewis and Elbe 1987) gas velocity, equivalence ratio, gas stream heterogeneity (Ahmed and Mastorakos 2006; Ballal and Lefebvre 1977, 1978; Lefebvre 1983), conditions of formation of a spherical flame kernel leading to a successful ignition (Champion, Deshaies, Joulin 1988; Champion et al. 1986; Deshaies and Joulin 1984), ignition probability in turbulent flows (Ahmed and Mastorakos 2006; Cordier et al. 2013; Neophytou,

Richardson, Mastorakos 2012), or effects of fuel spray characteristics (Ballal and Lefebvre 1981; Neophytou, Richardson, Mastorakos 2012). A recent review of forced ignition of spray flames is provided by Mastorakos (2017). Many experiments are available on the ignition of a single injector under a variety of conditions. Simulations have also been used to reproduce ignition processes, mainly again for a single sector. There is however one large scale simulation by Boileau et al. (2008) of the ignition sequence in an annular combustor comprising eighteen injectors but with no experimental validation. While many ignition correlations have been established from experiments on complete combustors, see for example Lefebvre (1983) or Naegli and Dodge (1991), there is a lack of detailed experimental data on the ignition and flame spreading in annular devices. The circular ignition of annular configurations is clearly less well documented than single injector configurations.

Ignition dynamics under premixed conditions

Data have become available from our recent work (Bourgouin et al., 2013b). Investigation of the light round mechanism has also been carried out in Cambridge (Bach et al. 2013; Machover and Mastorakos 2016, 2017). More recently another annular combustion facility has been developed with a design close to that of MICCA in China, see for example Xia et al. (2019).

The light round process taking place at the start of an annular system equipped with multiple swirling injectors is investigated in MICCA with the arrangement shown in Figure 3. The system comprises an upstream plenum closed at the top by a plate comprising sixteen swirling injectors and a combustion chamber made of two cylindrical concentric quartz tubes mounted on the annular plate which serves as a chamber backplane. The diameters of the inner and outer quartz tubes are 30 cm and 40 cm respectively. The length of the inner and outer tubes can be varied. It is set at 40 cm in the ignition experiments.

Air and propane are delivered to a premixing unit. The mixture is then conveyed to an annular plenum through eight channels which are plugged on the internal sides of this cavity. Gases in the plenum are injected into the combustion chamber through sixteen swirling injectors mounted on the flange which separates the plenum from the chamber

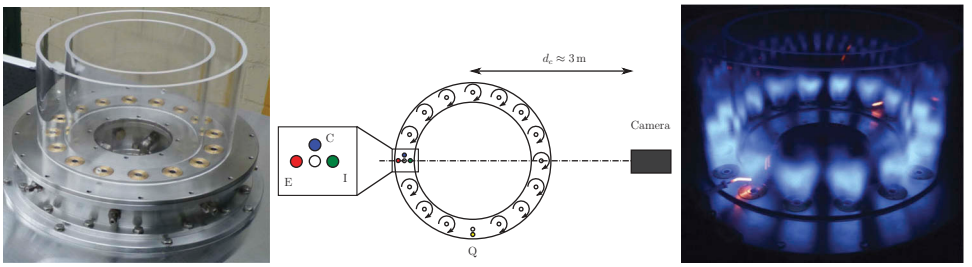

Figure 3. Left: view of the annular combustion chamber. The mean diameter of the ring is 350 mm. Two spark plugs are placed in diametrically opposite positions. Right: direct true color photograph of the swirling flames in the annular chamber equipped with the 200 mm quartz tubes under steady operation at a bulk velocity $v_0 = 19.6$ m.s^{-1} and an equivalence ratio $\phi = 0.76$ in each injection tube. The two diametrically opposed igniters can be seen in yellow/red due to their thermal radiation. Adapted from Bourgouin et al. (2013b). Originally published by ASME.

and constitutes the chamber backplane. Each injector is made of a cylindrical tube $D = 10$ mm in diameter at the bottom of which is placed a swirler equipped with nine blades to set the flow in rotation. The outlet section of the injector is flush mounted to the backplane of the combustion chamber which is cooled by an internal circulation of water. When viewed from above each swirling flow rotates in the clockwise direction.

The chamber walls are made of quartz allowing optical access to the flames and transmitting its radiation in the near ultraviolet and visible ranges. This provides a full access to the combustion region (Figure 3). Some reflections appear on the quartz tubes which form the combustor side walls. Figure 4 shows flame images recorded by the intensified CMOS camera during the propagation of the flame from the ignition kernel to the steady state operation. To improve the visualization, these images are plotted on a scale of colors where yellow corresponds to the highest intensity value while dark red represents the lowest value in flame emission. The igniter is placed in front of the camera on the opposite sector of the annular chamber. During the ignition process, the igniter generates a spark at a repetition rate of 100 Hz. The strong radiation of the spark plasma saturates some pixels of the camera sensor and it is not easy to distinguish the initial hot gas kernel, complicating the determination of the ignition instant. The initial pocket is convected by the flow and distorted by the local turbulent eddies. The delay associated with these various processes is around $\tau_0 \simeq 10$ ms. When the pocket meets favorable conditions, it expands and propagation becomes nearly isotropic and initially spherical. This defines the initial instant $t = 0$ in the following figures and it corresponds to a predefined

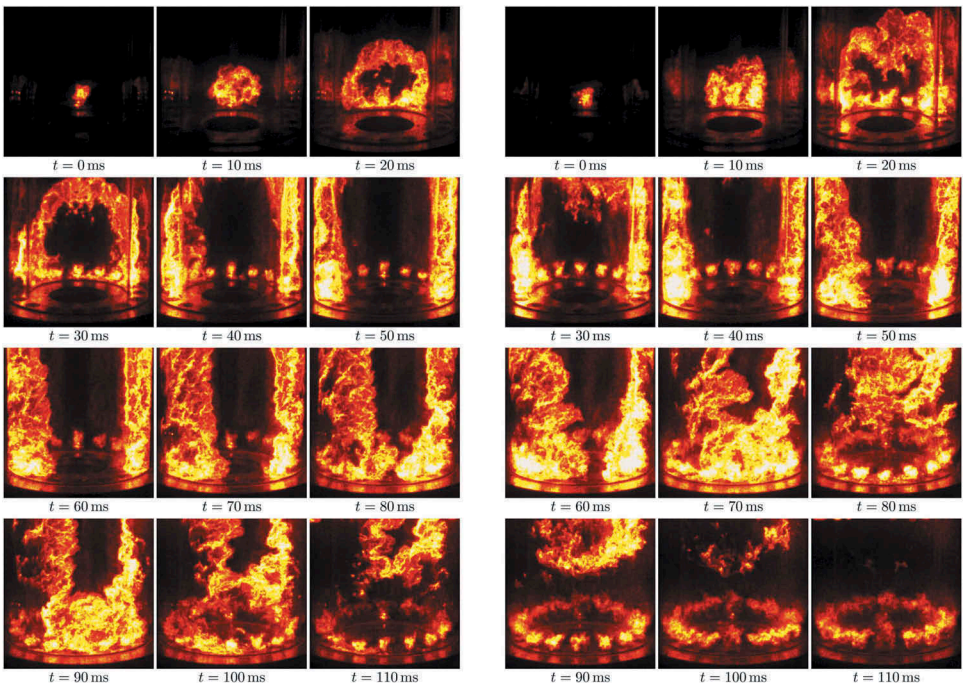

Figure 4. Images of light intensity emitted by the flame during an ignition of the annular chamber at $\phi = 0.76$. Left: $v_0 = 12.2$ m.s^{-1}. Right: $v_0 = 24.5$ m.s^{-1}. False colors are used to improve the visualization. Yellow and dark red respectively correspond to the highest and lowest values of light intensity. Adapted from Bourgouin et al. (2013b).

threshold intensity level. The flame then takes the shape of a symmetric arch at instant $t = 20$ ms. From $t = 40$ ms to $t = 70$ ms the two flame fronts are nearly vertical and the injectors are sequentially ignited by the propagating combustion front. The flame spreads more rapidly in the vicinity of the injectors and the two fronts begin to merge at time $t = 80$ ms and at a point that is not quite opposite to the igniter. The left side is in advance due to the swirl direction of rotation that induces a global gyration in the chamber. After merging of the left and right moving flame branches, the front is convected upwards by hot gases originating from the burners and the steady state is reached.

It is convenient to transform the images recorded by the camera to eliminate perspective effects by unwraping the cylindrical geometry of the system. This is accomplished in Figure 5. These images allow direct comparisons with simulations based on a level set description of flame propagation relying on turbulent velocity estimates (Bourgouin et al., 2013b).

It is also instructive to examine the global emission signal detected by the camera. This signal is representative of the heat release rate in the system. Figure 6 represents on the left the integrated light intensity for a bulk velocity $v_0 = 24.5$ m.s^{-1} and equivalence ratio $\phi = 0.76$. As explained previously a critical size c_s of the hot gas kernel is defined by an intensity threshold. This defines the instant $t = 0$ already used in Figure 4 to examine flame propagation. One can also define the delay τ_m from the time origin when the kernel size has reached c_s to the time where the left and right flame fronts merge. A final delay τ_p corresponds to the time duration between merging and steady state operation. The total propagation delay is then given by $\tau_t = \tau_m + \tau_p$. For a fixed value of the equivalence ratio, the steady state level is essentially proportional to the injection velocity v_0. This is coherent with the assumption that the camera signal can be qualitatively interpreted as proportional to the heat release rate. The recorded light intensity signals have a similar shape for all injection velocities explored. The frames where the fronts are merging can be manually selected and merging times τ_m can be deduced in this way as shown on the right in Figure 6.

Light round simulation and comparison with experiments

The MICCA experiments constitute an interesting case for testing the ability of large eddy simulation to retrieve data gathered during light round experiments. It is possible to compare time resolved flame visualizations with LES results obtained for the same multiple-injector annular combustor geometry and operating conditions. It is probably the first time that such

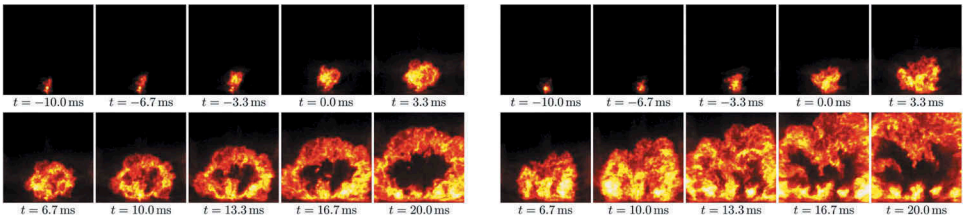

Figure 5. Numerically transformed images of light intensity emitted by the flame during an ignition of the annular chamber at $\phi = 0.76$. False colors are used to improve the visualization. Yellow and dark red respectively correspond to the highest and lowest values of light intensity. Left ten images: $v_0 = 12.2$ m.s^{-1}. Right ten images: $v_0 = 24.5$ m.s^{-1}. Adapted from Bourgouin et al. (2013b).

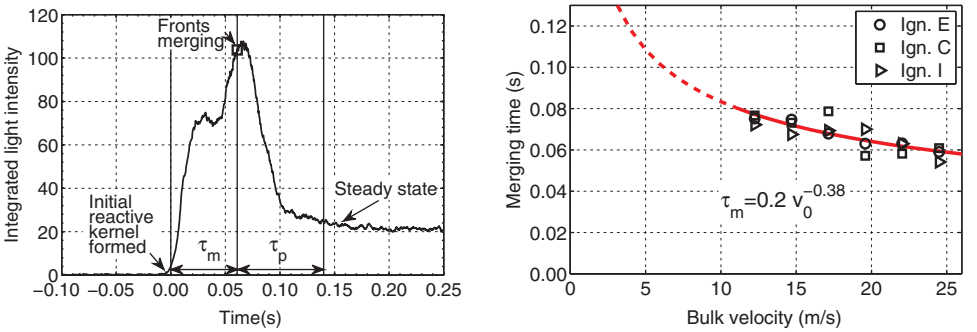

Figure 6. Left: Integrated light intensity recorded by the camera during ignition for a bulk velocity $v_0 = 24.5$ m.s^{-1}. The square symbols indicate the moment where the two flame fronts merge. Right: Propagation time τ_m for six flow rates and three igniter positions. Adapted from Bourgouin et al. (2013b).

a direct comparison was carried out for the light-round process (Figure 7). The comparison is illustrated by experimental data and calculations corresponding to an equivalence ratio $\phi = 0.76$ and a bulk velocity $U_b = 24$ m.s^{-1}. The experimental data is recorded with a high-speed intensified imaging CMOS camera at a frame rate of 6000 Hz and an exposition of 166 μs. This suitably resolves the flame during the light-round process which takes of the order of 50 ms. Calculations are carried-out with the AVBP flow solver, a code jointly developed by Cerfacs and IFP Energies Nouvelles together with the TACLES model derived in our laboratory to represent the chemical conversion in the LES framework. The computational domain comprises the upstream air and fuel manifolds, plenum, injectors and the annular chamber formed by the combustor backplane and quartz walls. The ambient atmosphere is represented by a large volume added at the exit of the combustor. The mesh comprises 310 million tetrahedra. The process is initiated by depositing a small sphere of burnt gases at the adiabatic flame temperature that is located at the position of the experimental spark ignitor. Further details and analysis may be found in Philip et al. (2014, 2015).

Figure 7 shows experimental data in the form of light emission images while numerical results are plotted as an isosurface of temperature colored by values of axial velocity. The structure of the flame brush at the largest scales is close to that observed experimentally, the instantaneous geometries of the flame front resemble those recorded by the high speed camera while the transit times from one injector to the next are quite similar, indicating that the LES with the selected sub-models suitably retrieves essential features of the light round process.

It is also interesting to examine the flame merging delays that are measured and simulated. Figure 8 shows data sets obtained under cold wall conditions and under preheated conditions. One notices that the thermal conditions at the walls have a notable influence on the propagation of the flame during the light round and on the value of the merging delay. The merging delay is longer when the chamber walls are initially cold. Preheated conditions are closest to the adiabatic wall boundary conditions used in the simulations. There is a good agreement between experimental data and the two calculated values of the merging delay.

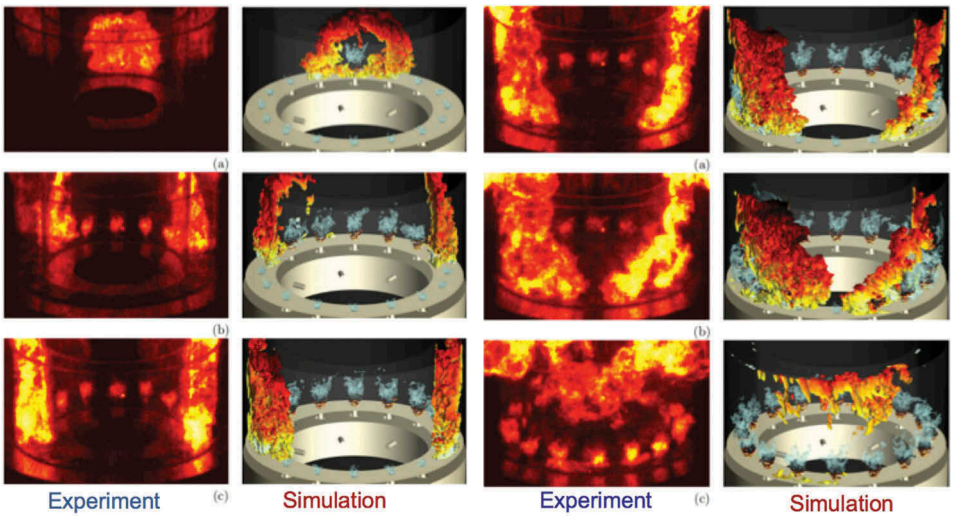

Figure 7. Light round ignition of the MICCA combustor. Experiment and simulation. $U_b = 24$ m s^{-1}, $\phi = 0.76$. These calculation are carried out in the configuration explored by Philip et al. (2015) but correspond to a higher value of the injection velocity U_b.

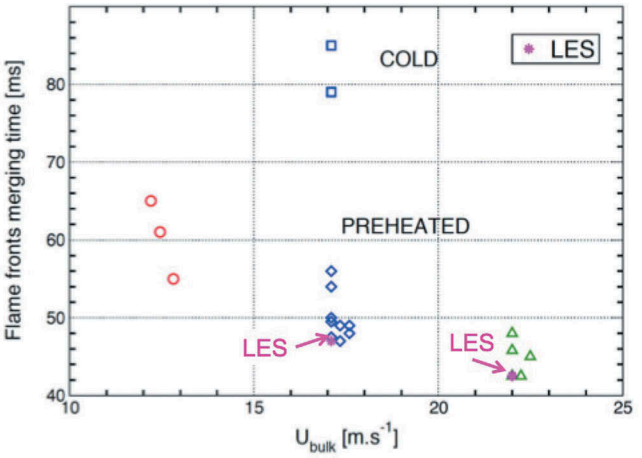

Figure 8. Flame merging delay plotted as a function of the bulk injection velocities. The red circles, blue diamonds and green triangles are obtained from experiments in which the chamber walls are preheated. The blue squares correspond to experiments under cold wall conditions. The calculated merging delays are shown as magenta star symbols. Adapted from Philip et al. (2015). Originally published by ASME.

Ignition dynamics under liquid spray injection

It is finally interesting to examine the characteristics of light round when the injection takes place in liquid form. This is accomplished by making use of a modified version of the annular combustor designated as MICCA-Spray. The liquid fuel heptane or dodecane is injected as a spray formed by hollow cone atomizers. Prieur et al. (2017a) compared the impact of the type

of combustion, premixed or spray, and the influence of fuel volatility. The process was extensively characterized with high-speed measurements with an intensified camera, photo-multipliers and microphone arrays placed in the plenum and in the chamber of the annular combustor. A large set of data is acquired and compared when the bulk velocity, the equivalence ratio or the power are varied. An example is given in Figure 9.

It is found that spray combustion does not affect the basic mechanisms of the light-round. The major effect of the fuel type is to modify the delay time τ_m that is found to decrease when the volatility of the fuel is augmented and that is further decreased when fuel and oxidizer are premixed. A close-up view on the behavior of the flame propagation in an arch-like pattern is shown in Figure 9. Detailed imaging of the passing flame front gives indications on the flame wrinkling. By recording the Mie scattering of the n-heptane droplets illuminated by a laser sheet, it is possible using particle image velocimetry (PIV) to observe the influence of the traveling flame front on the droplet distribution in the chamber. It is found that the propagating flame displaces the droplet spray well before the flame reaches the injector (Prieur et al. 2019). Using a similar technique, the traveling velocity of the flame front can be estimated. Large eddy simulations of the light round under liquid spray injection has also been explored (Lancien et al. 2018, 2019).

Further experiments have been concerned with the processes of injector initiation during the light round. Once ignited, each injector features a transient flame shape. The injector responds to the rapid change in heat release rate as it is initiated (Prieur et al. 2019). This produces a sudden drop in the air flow rate followed by a series of oscillations that correspond to a ringing of the injection unit when it is impulsively submitted to a sudden pressure increase in the chamber. Figure 10 illustrates on a single injector experiment how the flame evolves in time as a result of this initial drop in flow velocity and then under the influence of the dynamics of recirculation regions formed by the injection unit and corresponding changes in thermal conditions in the recirculation regions that are formed near the backplane. After a relatively long delay of the order of 30 ms the flame finds its final position above the injector.

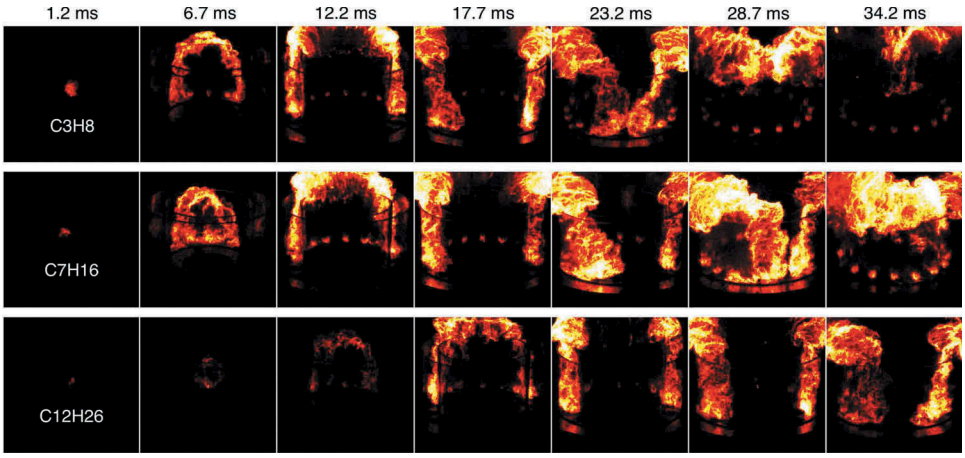

Figure 9. Light emission during the light round ignition sequence of propane (top), n-heptane (middle row) and dodecane (bottom row) fuels. Yellow corresponds to high light intensity while dark red represents low light emission. Injection conditions: U_b = 31.5 m s^{-1}, ϕ = 0.90 and $\mathcal{P}$= 80 kW. Adapted from Prieur et al. (2017a).

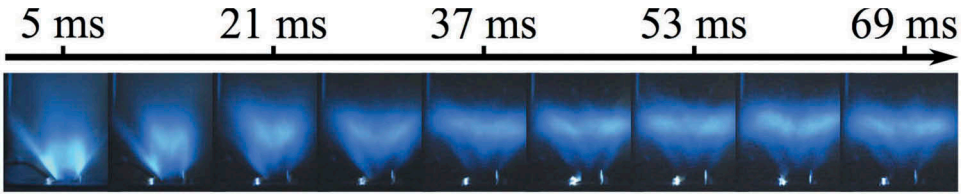

Figure 10. True-color ignition sequences in SICCA-spray.: U_b = 31 m s^{-1}, ϕ = 0.89 and $\mathcal{P}$= 80 kW. Adapted from Prieur et al. (2019). Originally published by ASME.

The injector dynamics can be represented by a differential model equation describing the response of this device and its recovery. The flame return to steady state is best retrieved by detailed large eddy simulations that suitably represent the thermal time scales that control the process which finally leads to an established flame (Töpperwien et al. 2019).

Experimental methodology for combustion instability analysis

Experiments on annular configurations are possible but both for the atmospheric rigs MICCA at EM2C and the Cambridge combustor of Dawson and Worth, a major challenge was to design injectors and confinement geometries giving rise to combustion instabilities coupled by azimuthal modes. It was quickly found that some guiding ideas were needed about injector geometry selection. This guidance may be obtained from simulations or perhaps from single sector experiments providing information on the flame response through measurements of the flame describing function. The objective was to determine the gain and phase that could be used with a theoretical model to predict instability. The combination of single sector and multiple injector annular combustor testing is represented in Figure 11.

Results of single sector experiments are illustrated in Figure 12. In this case the injector is fitted with a conical "cup". Experiments carried out for different cup angles indicate that the flame geometry notably changes as the cup angle is augmented. This is also reflected in the flame describing functions with some notable modifications of the gain and phase of these functions. This information could then be used in combination with a simplified theoretical framework to define the geometry giving access to instabilities in the annular chamber. The single sector experiments can thus be used to tailor the injector response in an iterative process. From an industrial point of view, the aim is of course just the opposite as one wishes to avoid naturally excited instabilities. The idea is then to work on the single sector configuration and, with the help of the theoretical framework, try to design an injector that will be less receptive to oscillations when arranged in an annular combustor system.

Combustion instabilities of premixed annular systems

Before reviewing experimental data concerning instabilities it is first useful to examine the acoustic modes of annular devices. This will be done in the next subsection by considering an idealized geometry. We will then successively review work on annular systems

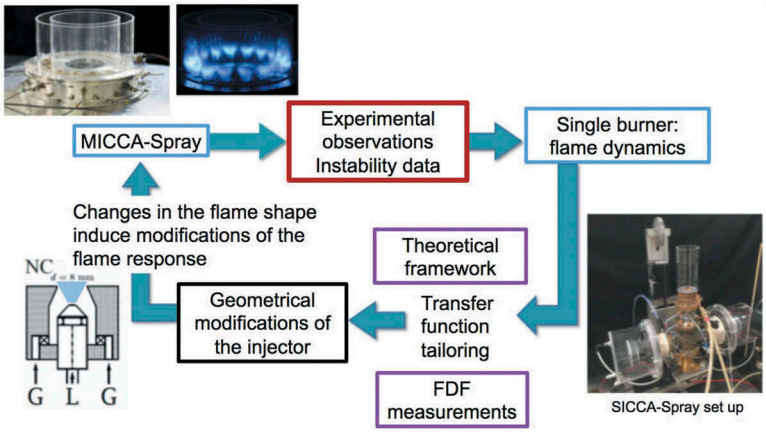

Figure 11. Experimental methodology combining single sector measurements in the SICCA setup and annular combustor testing on MICCA.

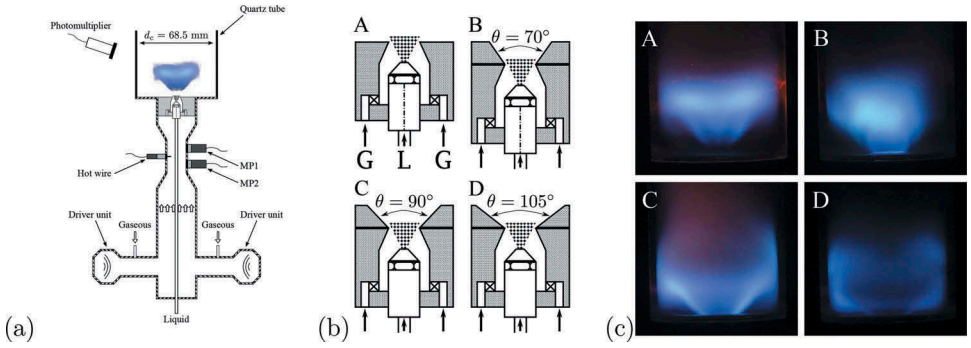

Figure 12. (a) Schematic of the burner to determine the flame response. (b) Injector configurations. Case A: No cup is installed. Case B: a 70° cup is installed. Case C: a 90° cup is installed. Case D: a 105° cup is installed. G stands for gas and L for liquid. (c) Flame shapes with different injector configurations. Case A: injector without cup generates an M flame. Case B: injector with 70° cup generates an amphora flame. Case C: injector with 90° cup generates a V flame. Case D: injector with 105° cup generates a corner flame.

equipped with swirling injectors featuring an outlet cup and an annular configuration comprising multiple matrix injection units.

Modal structures in annular chambers

The following discussion is concerned with the three configurations shown in Figure 13. The first of these geometries (Figure 13a) is formed by a cylindrical chamber with lateral walls of equal length l. The annular spacing and mean annular radius are d and R respectively. To be consistent with the conditions of the MICCA setup one may assume

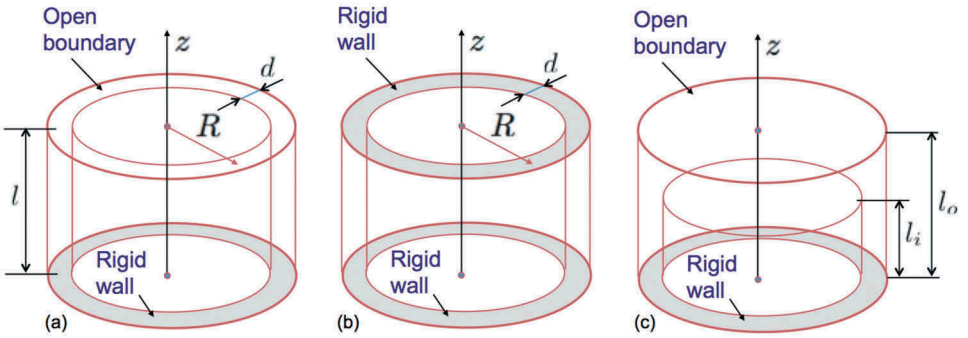

Figure 13. Annular geometries. (a) Annular chamber with a rigid backplane, equal length side walls and an open boundary, (b) Annular chamber with a rigid backplane and a rigid wall boundary condition at the outlet, (c) Annular chamber with unequal side walls.

that the bottom plane and side walls are rigid while the exhaust section is open to the atmosphere and corresponds to a pressure node. In fact the node is not exactly in the open section but at a distance from the outlet. One may assume for simplicity that this additional distance can be neglected. In practice this end correction is easily determined experimentally and can be added to the combustor length to improve the resonance frequencies estimations. To obtain simple analytical expressions it is also assumed that the sound velocity c is constant inside the system. It is also convenient to consider that the annular distance between the side walls is small compared to the mean diameter ($d << D = 2R$). One may then assume that the pressure waves in this configuration do not depend on the radial coordinate. Harmonic waves then satisfy a simplified Helmholtz equation:

$$\frac{1}{R^2}\frac{\partial^2 p}{\partial \theta^2} + \frac{\partial^2 p}{\partial z^2} + \frac{\omega^2}{c^2} p = 0 \tag{1}$$

This equation features purely azimuthal modes:

$$\psi_n(\theta) = a_n \exp(in\theta) + b_n \exp(-in\theta) \tag{2}$$

where a_n, b_n are constant amplitudes and the corresponding angular frequencies are $\omega_n = nc/R$ where n is an integer. The eigenfrequencies are then given by $f_n = nc/\mathcal{P}$ where $\mathcal{P} = 2\pi R$ is the mean perimeter of this annular configuration and the pressures waves take the form:

$$p_n(\theta, t) = a_n \exp(in\theta - i\omega_n t) + b_n \exp(-in\theta - i\omega_n t) \tag{3}$$

The pressure appears as a combination of a wave propagating in the positive azimuthal direction and a wave propagating in the negative azimuthal direction. These two waves respectively travel counter-clockwise and clockwise. There are also purely axial modes which for the rigid bottom plane – open outlet take the form:

$$\psi_m(z) = a_m \cos(k_m z) \tag{4}$$

where $k_m = (m - 1/2)\pi/l$ where m is an integer. The angular frequencies are then of the form $\omega_m = (m - 1/2)\pi(c/l)$ and the corresponding eigenfrequencies ar such that $f_m = (2m - 1)(c/4l)$. The annular geometry with a rigid backplane and an open outlet only sustains mixed modes which satisfy all boundary conditions. The corresponding eigenfunctions are a combination of those given previously:

$$\psi_{mn} = [a_n \exp(in\theta) + b_n \exp(-in\theta)] \cos(k_m z) \tag{5}$$

and the corresponding eigenfrequencies are:

$$f_{mn} = \left[(2m-1)^2 \left(\frac{c}{4l}\right)^2 + n^2 \left(\frac{c}{\mathcal{P}}\right)^2 \right]^{1/2} \tag{6}$$

The lowest eigenfrequency corresponds to $m = 1$ and $n = 0$: $f_{10} = c/(4l)$. This eigenfrequency is that of the first (quarter wave) axial mode (1L). The next eigenfrequency pertains to the first azimuthal -first axial mode 1A1L: $f_{11} = [(c/4l)^2 + (c/\mathcal{P})^2]^{1/2}$. When the length l is large, the first term in this expression becomes small and this eigenfrequency tends to $c/\mathcal{P}$ which characterizes the first azimuthal mode. In the experiments carried out in MICCA2, i.e. premixed conditions with swirling injectors fitted with a cup as shown in Figure 2-center and in MICCA-Spray, combustion oscillations are essentially coupled by the 1L and by the 1A1L modes of the chamber. The 1A1L mode features the 1A azimuthal structure that is of central interest. In experiments carried out with MICCA3 in premixed conditions with matrix injectors as shown in Figure 2-right, the coupling involves the plenum through a 1A1L mode and the corresponding eigenfrequency takes a lower value because the sound velocity in the plenum is also lower than in the chamber.

It was noted by a reviewer that the open end used in experimental facilities like MICCA does not quite represent the situation encountered in practical combustors where the chamber exhaust is formed by the turbine distributor which is generally choked. This imposes a choked nozzle boundary condition which may be approximated by an acoustically rigid wall condition sketched in Figure 13b. In this situation the system features purely azimuthal modes (1A, 2A …) with eigenfrequencies $f_n = nc/\mathcal{P}$. This is less easy to reproduce in the laboratory because it requires operation under pressurized conditions. However, it is possible to approach this situation by augmenting the length of the combustor to reduce the axial contribution to the resonant frequency of the mixed mode. For example the frequency of the 1A1L mode is only 11% greater than the frequency of the 1A mode if the perimeter to length ratio is equal to 2. This explains why in many experiments carried out in MICCA the combustor has at least 0.5 m in length.

In the third configuration shown in Figure 13c the sidewalls have unequal heights. This was used by (Worth and Dawson 2013a, 2013b) to obtain unstable regimes of operation as their experiments using walls with equal heights did not give rise to unstable oscillations. Similarly many experiments at EM2C were carried out with unequal wall heights. The question about the effect of this arrangement and its influence on stability is not yet fully settled but it is considered that this allows some mixing between the cool central stream of

air and the burnt products which tends to reduce the speed of sound in the upper part of the annulus. This is subsequently translated into a reduction in the eigenfrequencies corresponding to the acoustic modes in the system. This may then shift the resonant frequency in the range where the flame is sensitive to incoming perturbations. The corresponding augmentation in the flame response gain may be sufficient to move the operating conditions into an unstable region.

Experiments with premixed swirl injection

The annular system is now employed to investigate instability issues and specifically those involving azimuthal chamber modes. The inner and outer tubes lengths are 200 and 400 mm respectively. The swirling injectors are equipped with 90° cups that are flush mounted in the chamber backplane. This system features a strong longitudinal combustion instability for $v_0 = 20$ m.s^{-1} and $\phi = 0.79$. This is characterized by an intense emission of sound. Figure 14a shows that the five microphones exhibit a strong sinusoidal signal at a frequency $f = 252$ Hz and an amplitude $p_l = 330$ Pa. A harmonic is present at a frequency $f = 504$ Hz but with a significantly lower level (−25 dB). The pressure amplitude of the instability slowly varies in time in most cases between 280 Pa and 380 Pa. To extract the heat release rate oscillation pattern from the high-speed images, a dynamic mode decomposition (DMD) is used. This method introduced by Schmid (2010) relies on a large number of instantaneous images to extract a meaningful representation of the unsteady flow dynamics. It differs from the well-known proper orthogonal decomposition in that it is frequency selective. The camera records 12500 images per second corresponding to 49 images during one period of the instability. By processing 300 images at this sampling rate, one only has access to 6 periods. A value of about 20 periods would yield a better signal-to-noise ratio. This condition can be fulfilled by using only one image out of three in the calculation of the DMD modes. By processing 300 images, 18 periods are then considered with around 16 images per period. The DMD yields a frequency $f = 252$ Hz which is close to that detected by the microphones. The DMD modes are presented in Figure 14c,e,g,i which respectively pertain to the phases $\psi = 0$, $\psi = \pi/2$, $\psi = \pi$, and $\psi = 3\pi/2$. The phase $\psi = 0$ corresponds to the instant in the cycle where the maximum of heat release rate is reached. The flames are globally moving in phase and their motion is essentially that of a bulk oscillation. Some flames are desynchronized and two of them are even pulsating in phase opposition. The swirlers have been checked and no differences in the geometry have been observed. However, the flow dynamics downstream the swirlers is sensitive to the swirler geometries and even small differences in geometries can cause significant differences (Bourgouin et al., 2013c). Hydrodynamic instabilities in the plenum could also break the symmetry of the flow injection but their identification is not easy to perform. This dynamic mode decomposition also indicates that even if some flames are desynchronized, strong thermoacoustic instabilities can still occur in the chamber. The detuning imposed by these flames is not sufficiently effective to suppress the instability.

The study of azimuthal modes is more complicated because these modes are degenerate. An azimuthal mode can be interpreted as a superposition of clockwise and counterclockwise rotating components as indicated in Section 4.1. In the present study, the pressure amplitudes

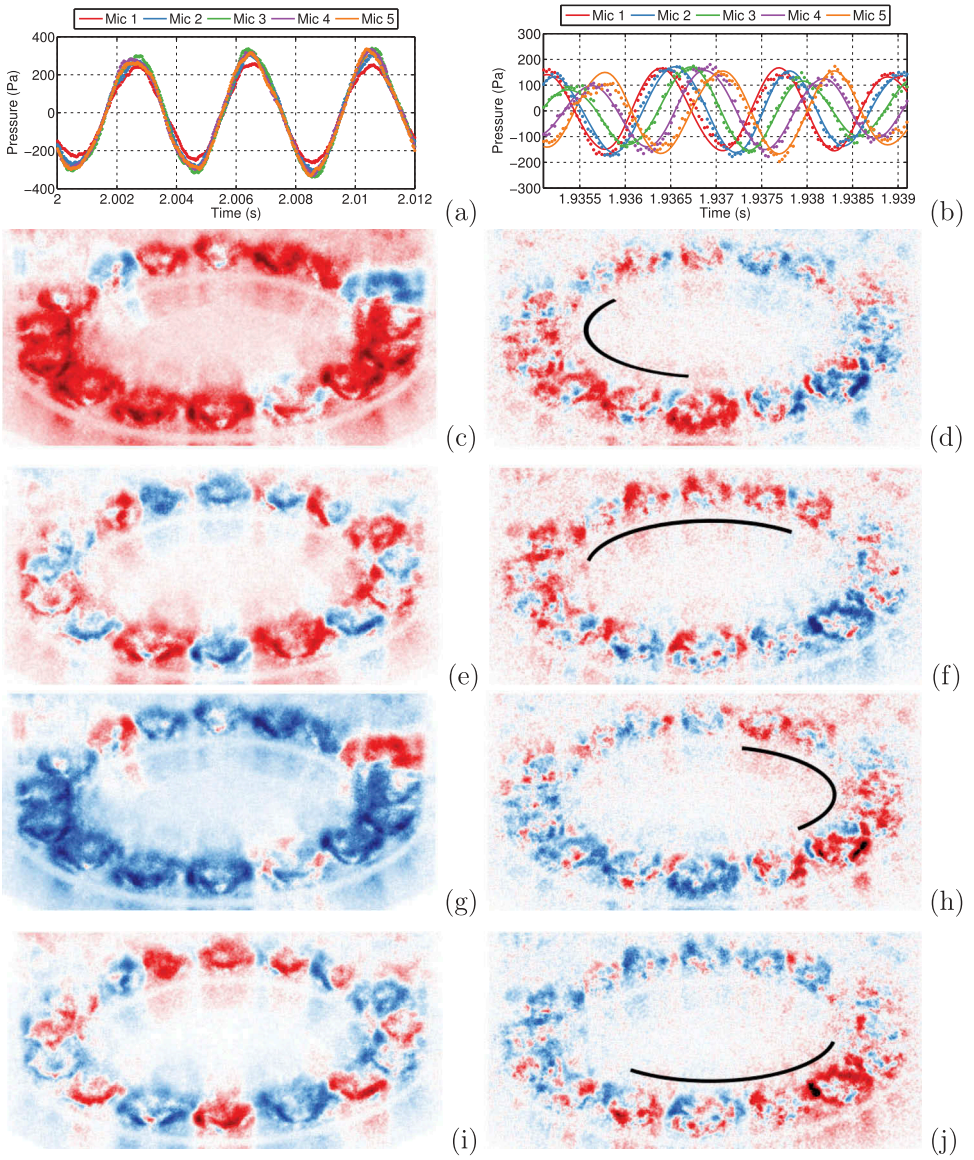

Figure 14. Pressure signals recorded by microphones (a, longitudinal oscillation) and (b, azimuthal spinning oscillation). In (b) the continuous lines correspond to the reconstructed signals. (c), (e), (g), (i): Dynamic mode decomposition (DMD) of 300 images recorded by the ICMOS camera for different phases for the longitudinal mode coupling at 252 Hz. (d),(f), (h), (j): Dynamic mode decomposition (DMD) of 300 images recorded by the ICMOS camera for different phases for an azimuthal mode coupling at 792 Hz. The mode is essentially rotating ($0.6 < s < 1.0$, see Eq. 8). The black curves indicate regions where the heat release rate is maximum. Adapted from Bourgouin et al. (2013b). Originally published by ASME.

recorded by the microphones are not constant in time in Figure 14b and the modal structure is also varying. The clockwise and counterclockwise wave components are varying in time as well, a feature that is also found by Worth and Dawson (2013a).

The clockwise and counterclockwise amplitudes may be deduced from the microphone signals. This is briefly explained in what follows. Near the backplane of the combustion chamber the acoustic pressure distribution only depends on the azimuthal angle θ and may be written as the sum of two waves:

$$p(\theta, t) = a\exp(i\theta - i\omega t) + b\exp(-i\theta - i\omega t) \tag{7}$$

Here a and b are respectively the complex amplitudes of the counterclockwise and clockwise rotating waves. When $b = 0$ the mode is counterclockwise, when $a = 0$, the mode is clockwise. When $|a| = |b|$ the mode is standing. Otherwise, the mode is neither purely rotating nor standing. The nature of the mode may be characterized in terms of a spin ratio:

$$s = \frac{|a| - |b|}{|a| + |b|} \tag{8}$$

The spin ratio s is such that $s = -1$, $s = 0$ and $s = 1$ respectively correspond to clockwise rotating, standing and counterclockwise rotating modes.

The pressure amplitudes of the five microphones are similar and there is a phase shift of about $\pi/8$ between each microphone in Figure 14b. The signals recorded by the microphones suggest that the mode is rotating clockwise. This is confirmed by the determination of the spin ratio which varies between $-1 < s < -0.6$ with a mean spin ratio $\bar{s} = -0.8$. As a result, the mode is essentially rotating in the clockwise direction. The DMD represented in Figure 14d,f,h,j also indicates a clockwise rotating motion which is consistent with the microphones signals. It is interesting to note that the DMD applied to a relatively short sequence reliably reconstructs standing and rotating modes. The azimuthal coupling described previously takes place at a relatively high frequency of 792 Hz corresponding to the 1A1 L mode of the chamber. One may then ask whether the swirling flames established in the system are sufficiently receptive to perturbations in this frequency range. Swirling flames are generally sensitive to low frequency perturbations. However the frequency extent of this range scales like the exhaust velocity and like the inverse of a typical flame dimension. The gain of the FDF may still take large values at Strouhal numbers of the order of one. For an exhaust velocity of 40 m/s and a typical flame size of about 4 cm, the sensitive range of frequencies will reach 1 kHz and which includes the resonance frequency of the 1A1 L mode. This is confirmed by measurements of the FDF in the single sector set up which indicate that the gain takes sizable values in a range extending to 850 Hz. In addition to this, the occurence of instability will also require conditions on the phase of heat release with respect to the pressure perturbation. The analysis of the modes identified in these experiments is carried out in further detail in Bourgouin et al. (2013b, 2015b).

The data gathered by Worth and Dawson (2013b) using the set up shown in Figure 1 also features some interesting rotating mode patterns. These are obtained by high speed imaging with a miror set at 45° from the combustor axis allowing a direct view of the annular flame arrangement. The camera operates at 14400 fps and detects OH* emission from the flames allowing a suitable sampling of oscillations taking place at a frequency $f \simeq 1700$ Hz which corresponds to a 1A1L mode. The resonant coupling takes place at a frequency that is about

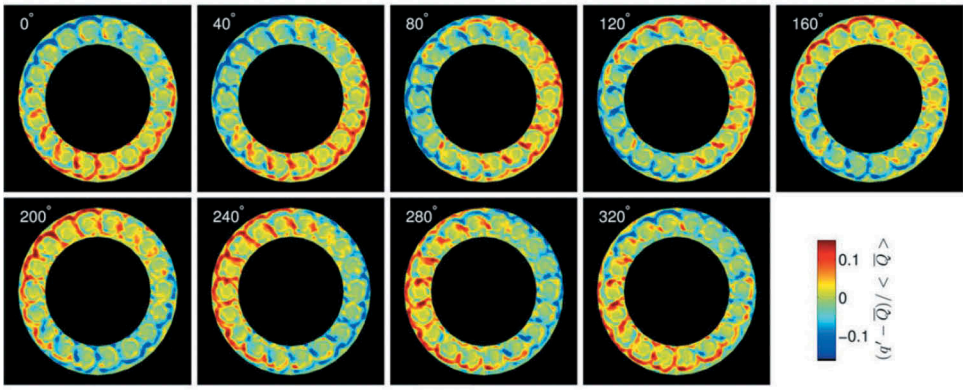

Figure 15. Circumferential mode spinning in the counter-clockwise direction. OH* emission is detected by a camera operating at 14,400 fps. The fluctuating light intensisty reflecting the heat release rate fluctutations is phase averaged. The patterns correspond to nine phases in a cycle. The system is fed with a mixture of air and ethylene at an equivalence ratio $\phi = 0.85$. Spacing between successive injectors $S/D = 1.56$. Reproduced from Worth and Dawson (2013b).

double that found in MICCA because the diameter of the system is about half that of MICCA. The circumferential spinning mode displayed in Figure 15 rotates in the counter-clockwise direction.

Studies carried out in various configurations as well as theoretical investigations indicate that azimuthal coupling modes in turbulent annular systems vary with time, leading to intermittent switching between predominantly spinning or standing states with changes in orientation of the modes Ghirardo and Juniper (2013); Noiray, Bothien, and Schuermans (2011); Worth and Dawson (2013b). Using loudspeakers, it was shown by Worth et al. (2017) and by Nygard et al. (2019) that the modes could be controlled easing the analysis of the combustion dynamics during clock wise spinning (CW, $s = -1$), anti-clockwise (ACW, $s = 1$) or standing azimuthal modes ($s = 0$). These studies were used to infer the importance of local swirl direction and the role of the separation distance between the injectors on the local flame structure and its response to the flow perturbations when coupled to azimuthal modes. Figure 16 reproduced from Nygard et al. (2019) is an example where CW, ACW and standing modes could be triggered for the same operating conditions by forcing the system at $f_0 = 1690$ Hz.

Premixed matrix injectors

The swirling injectors induce a complex flow pattern in the annular combustor. It is then natural to try to reduce the complexity of the flow and for that replace the swirling units by matrix injectors establishing multiple conical flames and operating in a laminar regime. This configuration (Figure 17) allows investigations of azimuthal coupling in the absence of swirl and turbulent fluctuations. In this new configuration it has been possible to examine stable limit cycles corresponding to a standing mode or to a rotating mode. It was also found that in a certain region of the domain of operation, designated as the *"dual mode"* region, the two types of modes could occur for the same operating conditions (Prieur et al. (2017b)).

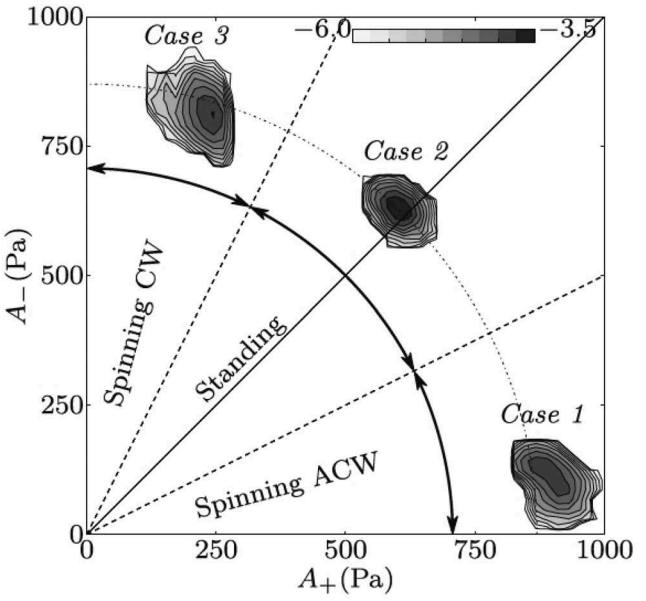

Figure 16. Joint PDF of the azimuthal wave amplitudes A_+ and A respectively corresponding to a and b in.Eq. (7) for three different cases, all using a forcing frequency $f_0 = 1690$ Hz. Dashed lines indicate $s = \pm 1/3$ and the solid line corresponds to $s = 0$. Case 1: $s = 0.9$. Case 2: $s = 0.0$. Case 3: $s = -0.6$. Reproduced from Nygard et al. (2019).

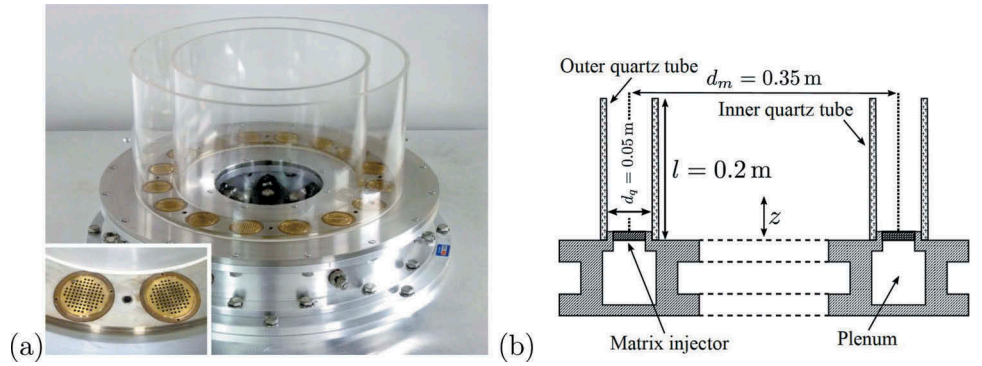

Figure 17. (a) Photograph of the MICCA3 chamber equipped with matrix injectors. The injectors comprise 89 holes of 2 mm diameter spaced by 3 mm. The thickness of the injector plate is fixed to 6 mm. The chamber formed by two cylindrical quartz tubes provides optical access to the flame region. (b) Lateral view of MICCA3. The length of the inner and outer quartz tubes are equal to $l = 0.2$ m, $d_q = 0.05$ m is the gap between the two quartz tubes and $d_m = 0.35$ m is the mean chamber diameter.

In that special region the nature of the oscillation depends on the path taken to reach the operating point (U_b, ϕ). If the equivalence ratio ϕ is increased, with the same air mass flow rate, from lean conditions to the target value, a rotating mode is obtained. If ϕ is decreased from rich conditions, a standing mode is manifested at the target conditions.

The rotating and standing modes do not switch from one to the other but instead when a mode arises, it is locked on. This experiment indicates that the nature of the mode (standing or spinning) is not only defined by the geometry or by some characteristics of the unstable regime but is also influenced by the history or more precisely by the path taken to reach the nominal operating point.

Combustion instabilities of annular systems equipped with swirl spray injectors

Liquid fuel injection adds further complexity to experimentation and modeling but is nevertheless interesting because it comes closer to practical situations like those found in aeroengines where kerosene is introduced in the combustor as a spray of droplets. The annular combustor was fitted with a set of swirl spray injectors shown in Figure 18 in a configuration designated as MICCA-Spray. This has allowed an examination of combustion instabilities coupled by azimuthal modes. The system is sufficiently flexible to allow investigations under fully premixed gaseous, liquid heptane and liquid dodecane injection. The single sector test bed (SICCA) was also modified to accommodate liquid injection. Systematic investigations have been carried out with a series of swirlers designed to have the same swirl number but different head loss levels (Vignat et al. 2019). It was found that changes in the head loss had a notable influence on the unstable oscillations.

Among the many experiments carried out in MICCA-Spray, those yielding very large combustion instability levels coupled to the 1A1 L mode of the annular cavity have some unusual consequences. In many cases the oscillations take the form of long bursts with a repetition rate of approximately a few hertz. During these bursts, the acoustic pressure fluctuation can reach up to 6% of the ambient pressure in the chamber corresponding to a peak level of approximately 6000 Pa. The type of instability, that arises under these circumstances is investigated in detail in Prieur et al. (2018) and more recently in Vignat

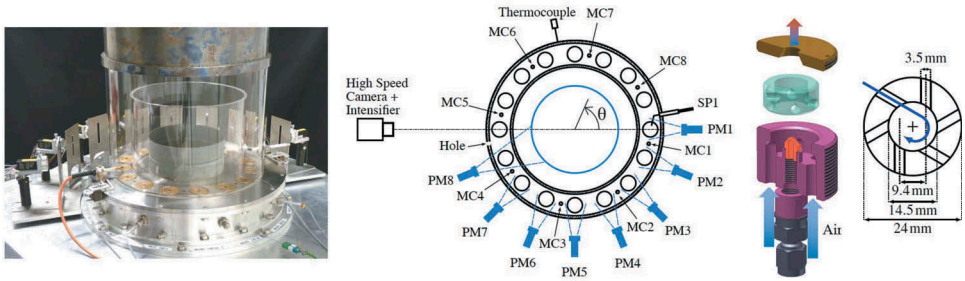

Figure 18. From left to right. From left to right: (1) Photograph of the MICCA-Spray test rig. (2) Schematic view of the chamber backplane showing the locations of the camera, thermocouple, chamber microphones MCx, plenum microphones MPx, photomultipliers PMx and of spark plug SP1. Dashed lines show the field of view of the photomultipliers. (3) Exploded view of the injector and its components. In purple, the main body, in orange the liquid fuel atomizer, in translucide teal the tangential air swirler and in gold the injector outlet, which is flush with the chamber backplane. (4) Schematic view of the swirler seen from above indicating the main dimensions of this component. From Vignat et al. (2020). Originally published by ASME.

et al. (2020). By determining the spin ratio one observes that this process occurs predominantly when the acoustic coupling mode is of the standing type.

Specific attention is given to the flame behavior at the nodal positions during the standing mode. Flames located in the neighborhood of this line are submitted to an intense transverse motion. When the pressure oscillation takes large values, the transverse velocity reaches a critical value which displaces the flow and disrupts the recirculation regions that stabilize the flame (Prieur et al., 2017a). The resulting flame dynamics is illustrated in Figures 19 and 20. Using a higher order reconstruction method for the pressure field it is possible to calculate the pressure distribution and determine the acoustic velocity field just before blow-off occurs Vignat et al. 2020. It is found that the pressure field is modified as the amplitude of the oscillation increases, leading to a distortion of the pressure distribution in the system that must be accounted for pressure

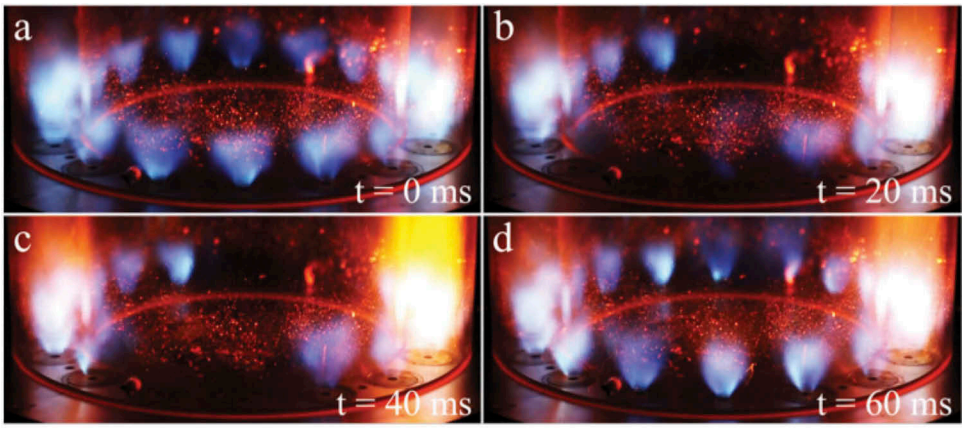

Figure 19. True-color photographs of the annular chamber when six flames are blown-off for about 20 ms. ϕ = 0.85, W=111 kW. From Prieur et al. (2018) originally published by ASME.

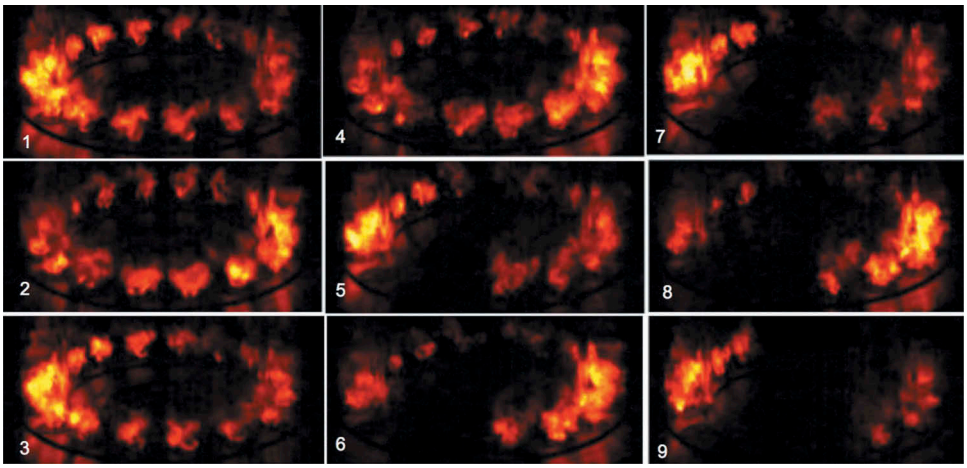

Figure 20. Sequence of 9 images illustrating the partial flame blow off in MICCA-Spray in the presence of an azimuthal standing mode of high amplitude (4000 Pa peak). $\phi = 0.85, \mathrm{W}{=}111$ kW.

field reconstruction and acoustic eigenfunction calculations. The critical value of the transverse velocity oscillation inducing blow-off is about 30% of the axial velocity at the injector exhaust. Flame blow-off can lead to the distortion of the pressure field, and also contributes to a decrease in the resonant frequency, a feature that is observed in the experiments.

Conclusions

This review is focused on dynamical issues raised by annular combustion systems found in most areo engines and modern gas turbines. Ignition dynamics and combustion instabilities coupled by azimuthal modes are specifically considered. It is argued that the corresponding processes cannot be investigated in single injector devices and need to be examined in annular configurations but it is also noted that experiments carried out in single sector geometries provide valuable information and are best exploited in combination with annular testing. The single sector experiments may be used to select injectors, determine their response to incident perturbations, obtain their describing functions and select geometries that will give rise to instabilities when they are tested in the annular geometry. Recent experiments in annular systems are exemplified. The light round process is investigated and characterized with high speed images of the flame providing information on the mechanisms controlling the flame dynamics. It is shown that data gathered in these experiments can serve to validate large eddy simulations of the light round process. Instability issues are then examined using the same annular setup in combination with single sector experiments. It is found that the system sustains axial and azimuthal-axial modes of oscillation. In the first case the flames respond essentially in phase with the pressure. In the latter case, the azimuthal mode is formed by two waves which yield various combinations of standing and rotating disturbances. Pressure data recorded by multiple microphones can be used to determine the complex amplitudes of waves traveling in the clockwise and counterclockwise directions, deduce a spin ratio and sort out the various modes appearing in the system. It is found that the spin ratio changes continuously during experiments and that the oscillations feature all possible combinations of the azimuthal components that rotate in the counterclockwise and clockwise directions. Experiments on an annular geometry featuring matrix injectors serve to show that it is possible to observe a standing or spinning mode for the same operating conditions and that the type of mode that arises depends on the path taken to reach the point of operation. Other experiments carried out with swirl spray injectors indicate that strong levels of oscillation are possible reaching a few kPa peak levels, corresponding to a - few percent of the chamber pressure, and that when this happens flames located near the pressure nodal line are extinguished. This process is accompanied by a sharp change in frequency and a notable distortion of the pressure distribution inside the chamber.

The many new results obtained indicate that it is worth pursuing investigations of annular geometries comprising multiple injectors in combination with single sector studies. The data gathered may be used to improve the state of understanding of the basic mechanisms controlling the light round and help design injectors that are less sensitive to dynamical perturbations. These data may also serve to guide the development of tools for simulation and prediction of dynamical phenomena like ignition or combustion instability coupled by azimuthal modes.

Acknowledgments

Support provided to this research by CNRS, CentraleSupelec, Université Paris Saclay, the Agence Nationale de la Recherche (MICCA ANR-08-BLAN-0027-01, FASMIC ANR-16-CE22-0013, and TIMBER ANR14-CE23-0009-01 projects), Safran, DGA and the European Union's Horizon 2020 research and innovation program (Grant 765998, Annulight) are gratefully acknowledged.

Disclosure Statement

No potential conflict of interest was reported by the authors.

Funding

This work was supported by the Agence Nationale de la Recherche [FASMIC ANR-16-CE22-0013, TIMBER ANR14-CE23-0009-01]; Safran [NF5Z-5100]; European Union's Horizon 2020 research and innovation program [Grant 765998, Annulight].

References

Ahmed, S. F., and E. Mastorakos. 2006. Spark ignition of lifted turbulent jet flames. *Combust. Flame* 146:215–31. doi:10.1016/j.combustflame.2006.03.007.

Bach, E., J. Kariuki, J. Dawson, E. Mastorakos, and H. Bauer. 2013. Spark ignition of single bluff-body premixed flames and annular combustors. AIAA paper. 2013–1182. Washington: American Institute of Aeronautics and Astronautics.

Ballal, D., and A. Lefebvre. 1974. The influence of flow parameters on minimum ignition energy and quenching distance. *Proc. Combust. Inst.* 15: 1473–81.

Ballal, D. R., and A. H. Lefebvre. 1977. Ignition and flame quenching in flowing gaseous mixtures. *Proc. R. Soc. London Ser. A* 357:163–81.

Ballal, D. R., and A. H. Lefebvre. 1978. Ignition and flame quenching of quiescent fuel mists. *Proc. R. Soc. London Ser. A* 364:277–94.

Ballal, D. R., and A. H. Lefebvre 1981. A general model of spark ignition for gaseous and liquid fuel-air mixtures. *Proc. Combus. Inst.* 18:1737–47

Bauerheim, M., J. F. Parmentier, P. Salas, F. Nicoud, and T. Poinsot. 2014a. An analytical model for azimuthal thermoacoustic modes in an annular chamber fed by an annular plenum. *Combust. Flame* 161:1374–89. doi:10.1016/j.combustflame.2013.11.014.

Bauerheim, M., P. Salas, F. Nicoud, and T. Poinsot. 2014b. Symmetry breaking of azimuthal thermo-acoustic modes in annular cavities: A theoretical study. *J. Fluid Mech.* 760:431–65. doi:10.1017/jfm.2014.578.

Boileau, M., G. Staffelbach, B. Cuenot, T. Poinsot, and C. Berat. 2008. LES of an ignition sequence in a gas turbine engine. *Combust. Flame* 154:2–22. doi:10.1016/j.combustflame.2008.02.006.

Borghesi, G., F. Biagioli, and B. Schuermans. 2009. Dynamic response of turbulent swirling flames to acoustic perturbations. *Combust. Theory Modell.* 13:487–512. doi:10.1080/13647830902829383.

Boudy, F., D. Durox, T. Schuller, and S. Candel. 2011. Nonlinear mode triggering in a multiple flame combustor. *Proc. Combust. Inst.* 33:1121–28.

Bourgouin, J. F., D. Durox, J. Moeck, T. Schuller, and S. Candel. 2013a. Self-sustained instabilities in an annular combustor coupled by azimuthal acoustic modes. GT2013-95010 ASME Turbo Expo 2013. New York: American Society of Mechanical Engineers.

Bourgouin, J. F., D. Durox, J. P. Moeck, T. Schuller, and S. Candel. 2015a. Characterization and modeling of a spinning thermoacoustic instability in an annular combustor equipped with multiple matrix injectors. *J. Eng. Gas Turbines Power* 137:021503 (11 pages). doi:10.1115/1.4028257.

Bourgouin, J. F., D. Durox, J. P. Moeck, T. Schuller, and S. Candel. 2015b. A new pattern of instability observed in an annular combustor: The slanted mode. *Proc. Combus. Inst.* 35:3237–44.
Bourgouin, J. F., D. Durox, T. Schuller, J. Beaunier, and S. Candel. 2013b. Ignition dynamics of an annular combustor equipped with multiple swirling injectors. *Combust. Flame* 160:1398–413. doi:10.1016/j.combustflame.2013.02.014.
Bourgouin, J. F., J. Moeck, D. Durox, T. Schuller, and S. Candel. 2013c. Sensitivity of swirling flows to small changes in the swirler geometry. *Comptes Rendus Mecanique* 341:211–19. doi:10.1016/j.crme.2012.10.018.
Candel, S. 2002. Combustion dynamics and control: Progress and challenges. *Proc. Combust. Inst.* 29:1–28.
Candel, S., D. Durox, T. Schuller, J. F. Bourgouin, and J. P. Moeck. 2014. Dynamics of swirling flames. *Annu. Rev. Fluid Mech.* 46:147–73. doi:10.1146/annurev-fluid-010313-141300.
Candel, S., M. Juniper, G. Singla, P. Scouflaire, and C. Rolon. 2006. Structure and dynamics of cryogenic flames at supercritical pressure. *Combust. Sci. Technol.* 178:161–92. doi:10.1080/00102200500292530.
Champion, M., B. Deshaies, G. Joulin, and K. Kinoshita. 1986. Spherical flame initiation: Theory versus experiments for lean propane-air mixtures. *Combust. Flame* 65:319–37. doi:10.1016/0010-2180(86)90045-3.
Champion, M., B. G. Deshaies, and G. Joulin. 1988. Relative influences of convective and diffusive transports during spherical flame initiation. *Combust. Flame* 74:161–70. doi:10.1016/0010-2180(88)90014-4.
Cordier, M., A. Vandel, G. Cabot, B. Renou, and A. Boukhalfa. 2013. Laser induced spark ignition of premixed confined swirling flames. *Combust. Sci. Technol.* 185:379–407. doi:10.1080/00102202.2012.725791.
Cosic, B., J. Moeck, and C. Paschereit. 2014. Nonlinear instability analysis for partially premixed swirl flames. *Combust. Sci. Technol.* 186:713–36. doi:10.1080/00102202.2013.876420.
Crocco, L. 1951. Aspects of combustion instability in liquid propellant rocket motors. part i. *J. Am. Rocket Soc.* 21:163–78. doi:10.2514/8.4393.
Crocco, L. 1952. Aspects of combustion instability in liquid propellant rocket motors. part ii. *J. Am. Rocket Soc.* 22:7–16. doi:10.2514/8.4410.
Crocco, L., and S. Cheng. 1953. High-frequency combustion instability in rocket motor with concentrated combustion. *J. Am. Rocket Soc.* 23:301. doi:10.2514/8.4623.
Crocco, L., and S. I. Cheng. 1956. *Theory of combustion instability in liquid propellant rocket motors*. Vol. Agardograph No. 8. New York: Butterworths Science.
Crocco, L. L., and W. Sirignano. 1966. Effect of transverse velocity component on nonlinear behavior of short nozzles. *AIAA J.* 4:1428. doi:10.2514/3.3691.
Culick, F. E. C. 2001. *Dynamics of combustion systems: Fundamentals, acoustics and control.* Cleveland: NASA Glenn Research Center.
Dawson, J. R., and N. A. Worth. 2014. Flame dynamics and unsteady heat release rate of self-excited azimuthal modes in an annular combustor. *Combust. Flame* 161:2565–78. doi:10.1016/j.combustflame.2014.03.021.
Dawson, J. R., and N. A. Worth. 2015. The effect of baffles on self-excited azimuthal modes in an annular combustor. *Proc. Combust. Inst.* 35:3283–90.
Deshaies, B., and G. Joulin. 1984. On the initiation of a spherical flame kernel. *Combust. Sci. Technol.* 37:99–116. doi:10.1080/00102208408923749.
Dowling, A. 1997. Nonlinear self-excited oscillations of a ducted flame. *J. Fluid Mech.* 346:271–90. doi:10.1017/S0022112097006484.
Dowling, A. P., and S. R. Stow. 2003. Acoustic analysis of gas turbine combustors. *J. Propul. Power* 19:751–64. doi:10.2514/2.6192.
Durox, D., J. P. Moeck, J. F. Bourgouin, P. Morenton, M. Viallon, T. Schuller, and S. Candel. 2013. Flame dynamics of a variable swirl number system and instability control. *Combust. Flame* 160:1729–42. doi:10.1016/j.combustflame.2013.03.004.

Durox, D., K. Prieur, T. Schuller, and S. Candel. 2016. Different flame patterns linked with swirling injector interactions in an annular combustor. *J. Eng. Gas Turbines Power* 138 doi:10.1115/1.4033330.

Evesque, S., W. Polifke, and C. Pankiewitz 2003. Spinning and azimuthally standing acoustic modes in annular combustors. In AIAA Conference Proceedings Paper 2003–3182, 9th AIAA/CEAS Aeroacoustics Conference, Hilton Head, South Carolina.

Fanaca, D., P. R. Alemela, C. Hirsch, and T. Sattelmayer. 2010. Comparison of the flow field of a swirl stabilized premixed burner in a annular and a single burner combustion chamber. *J. Eng. Gas Turbines Power* 132 (7):071502. doi:10.1115/1.4000120

Gatti, M., R. Gaudron, C. Mirat, L. Zimmer, and T. Schuller. 2019. Impact of swirl and bluff-body on the transfer function of premixed flames. *Proc. Combust. Inst.* 37:51977–5204.

Ghirardo, G., and M. P. Juniper 2013. Azimuthal instabilities in annular combustors: Standing and spinning modes. *Proc. R. Soc. A*. 469 20130232 doi:10.1098/rspa.2013.0232.

Ghirardo, G., M. P. Juniper, and J. P. Moeck. 2016. Weakly nonlinear analysis of thermoacoustic instabilities in annular combustors. *J. Fluid Mech.* 805:52–87. doi:10.1017/jfm.2016.494.

Gicquel, L., G. Staffelbach, and T. Poinsot. 2012. Large eddy simulations of gaseous flames in gas turbine combustion chambers. *Prog. Energy Combust. Sci.* 38:782–817. doi:10.1016/j.pecs.2012.04.004.

Hakim, L., A. Ruiz, T. Schmitt, M. Boileau, G. Staffelbach, S. Ducruix, B. Cuenot, and S. Candel. 2015a Large eddy simulations of multiple transcritical coaxial flames submitted to a high-frequency transverse acoustic modulation. *Proc. Combust. Inst.* 35:1461–68.

Hakim, L., T. Schmitt, S. Ducruix, and S. Candel. 2015b. Dynamics of a transcritical coaxial flame under a high-frequency transverse acoustic forcing: Influence of the modulation frequency on the flame response. *Combust. Flame* 162:3482–502. doi:10.1016/j.combustflame.2015.05.022.

Han, X., and A. Morgans. 2018. Non-linear interactions of two premixed flames explored by large eddy simulation with external acoustic forcing. *Combust. Sci. Technol.* 190:424–35. doi:10.1080/00102202.2017.1398148.

Harrje, D. J., and F. H. Reardon, eds. 1972. Liquid propellant rocket instability. Tech. Rep. Report SP-194. Washington, D.C: NASA.

Huang, Y., and V. Yang. 2009. Dynamics and stability of lean-premixed swirl-stabilized combustion. *Prog. Energy Combust. Sci.* 35:293–364. doi:10.1016/j.pecs.2009.01.002.

Juniper, M., A. Tripathi, P. Scouflaire, J. Rolon, and S. Candel 2000. Structure of cryogenic flames at elevated pressures. *Proc. Combust.Inst.* 28:1103–09

Komarek, T., and W. Polifke. 2010. Impact of swirl fluctuations on the flame response of a perfectly premixed swirl burner. *J. Eng. Gas Turbines Power* 132:061503 (7 pages). doi:10.1115/1.4000127.

Kopitz, J., A. Huber, T. Sattelmayer, and W. Polifke. 2005. Thermoacoustic stability analysis of an annular combustion chamber with acoustic low order modeling and validation against experiment. In ASME Conference Proceedings, Paper GT 2005-68797, ASME Turbo Expo, Reno-Tahoe, Nevada.

Krebs, W., P. Flohr, B. Prade, and S. Hoffmann. 2002. Thermoacoustic stability chart for high-intensity gas turbine combustion systems. *Combust. Sci. Technol.* 174:99–128. doi:10.1080/00102200208984089.

Laera, D., T. Schuller, K. Prieur, D. Durox, S. M. Camporeale, and S. Candel. 2017. Flame describing function analysis of spinning and standing modes in an annular combustor and comparison with experiments. *Combust. Flame* 184:136–52. doi:10.1016/j.combustflame.2017.05.021.

Lancien, T., K. Prieur, D. Durox, S. Candel, and R. Vicquelin. 2018. Large eddy simulation of light-round in an annular combustor with liquid spray injection and comparison with experiments. *J. Eng. Gas Turbines Power* 140:021504(10 pages). doi:10.1115/1.4037827.

Lancien, T., K. Prieur, D. Durox, S. Candel, and R. Vicquelin. 2019. Leading point behavior during the ignition of an annular combustor with liquid n-heptane injectors. *Proc. Combust. Inst.* 37:5021–29.

Lefebvre, A. H. 1983. *Gas turbines combustion*. New York, NY: McGraw Hill.

Lewis, B., and G. V. Elbe. 1987. *Combustion, flames and explosions of gases*. 3rd ed. New York, NY: Academic Press.
Lieuwen, T., H. Torres, C. Johnson, and B. T. Zinn. 2001. A mechanism of combustion instability in lean premixed gas turbine combustors. *J. Eng. Gas Turbines Power* 123:182–89. doi:10.1115/1.1339002.
Lieuwen, T., and V. Yang, eds. 2005. *Combustion instabilities in gas turbine engines, operational experience, fundamental mechanisms, and modeling*. Vol. 210 of *Progress in astronautics and aeronautics*. Washington, DC: American Institute of Aeronautics and Astronautics.
Machover, E., and E. Mastorakos. 2016. Spark ignition of annular non-premixed combustors. *Exp. Therm Fluid Sci.* 73:64–70. doi:10.1016/j.expthermflusci.2015.09.008.
Machover, E., and E. Mastorakos. 2017. Numerical investigation of the stochastic behavior of light-round in annular non-premixed combustors. *Combust. Sci. Technol.* 189:1467–85. doi:10.1080/00102202.2017.1305366.
Marble, F., and D. Cox. 1953. Servo-stabilization of low-frequency oscillations in a liquid bipropellant rocket motor. *J. Am. Rocket Soc.* 23:85. doi:10.2514/8.4542.
Mastorakos, E. 2017. Forced ignition of turbulent spray flames. *Proc. Combust. Inst.* 36:2367–83.
Mery, Y., L. Hakim, P. Scouflaire, L. Vingert, S. Ducruix, and S. Candel. 2013. Experimental investigation of cryogenic flame dynamics under transverse acoustic modulations. *C. R. Mec.* 341:100–09. doi:10.1016/j.crme.2012.10.013.
Mitchell, C., L. Crocco, and W. Sirignano. 1969. Nonlinear oscillations in liquid rocket combustion chambers. *Astronaut. Acta* 14:409.
Moeck, J. P., M. Paul, and C. O. Paschereit 2010. Thermoacoustic instabilities in an annular rijke tube. In ASME Conference Proceedings, Paper GT 2010-23577, ASME Turbo Expo, Glasgow, UK.
Naegli, D. W., and L. G. Dodge. 1991. Ignition study in a gas turbine combustor. *Combust. Sci. Technol.* 80:165–84. doi:10.1080/00102209108951784.
Neophytou, A., E. Richardson, and E. Mastorakos. 2012. Spark ignition of turbulent recirculating non-premixed gas and spray flames: A model for predicting ignition probability. *Combust. Flame* 159:1503–22. doi:10.1016/j.combustflame.2011.12.015.
Noiray, N., and B. Schuermans 2013. On the dynamic nature of azimuthal thermoacoustic modes in annular gas turbine combustion chambers. *Proc. R. Soc. A* 49: 20120535. doi:10.1098/rspa.2012.0535.
Noiray, N., D. Durox, T. Schuller, and S. Candel. 2008. A unified framework for nonlinear combustion instability analysis based on the flame describing function. *J. Fluid Mech.* 615:139–67. doi:10.1017/S0022112008003613.
Noiray, N., M. Bothien, and B. Schuermans. 2011. Investigation of azimuthal staging concepts in annular gas turbines. *Combust. Theory Modell.* 15:585–606. doi:10.1080/13647830.2011.552636.
Nygard, H., M. Mazur, J. R. Dawson, and N. Worth. 2019. Flame dynamics of azimuthal forced spinning and standing modes in an annular combustor. *Proc. Combust. Inst.* 37:5113–20.
O'Connor, J., V. Acharya, and T. Lieuwen. 2015. Transverse combustion instabilities: Acoustic, fluid mechanic, and flame processes. *Prog. Energy Combust. Sci.* 49:1–39. doi:10.1016/j.pecs.2015.01.001.
Palies, P., D. Durox, T. Schuller, and S. Candel. 2010. The combined dynamics of swirler and turbulent premixed swirling flames. *Combust. Flame* 157:1698–717. doi:10.1016/j.combustflame.2010.02.011.
Palies, P., D. Durox, T. Schuller, and S. Candel. 2011. Nonlinear combustion instabilities analysis based on the flame describing function applied to turbulent premixed swirling flames. *Combust. Flame* 158:1980–91. doi:10.1016/j.combustflame.2011.02.012.
Pankiewitz, C., and T. Sattelmayer. 2003. Time domain simulation of combustion instabilities in annular combustors. *J. Eng. Gas Turbines Power* 125:677–85. doi:10.1115/1.1582496.
Philip, M., M. Boileau, R. Vicquelin, T. Schmitt, D. Durox, J. F. Bourgouin, S. Candel. 2014. Ignition sequence of an annular multi-injector combustor. *Phys. Fluids* 26. doi:10.1063/1.4893452.

Philip, M., M. Boileau, R. Vicquelin, T. Schmitt, D. Durox, J. F. Bourgouin, S. Candel. 2015. Simulation of the ignition process in an annular multiple-injector combustor and comparison with experiments. *J. Eng. Gas Turbines Power* 137. doi:10.1115/1.4028265.

Poinsot, T. 2017. Prediction and control of combustion instabilities in real engines. *Proc. Combust. Inst.* 36:1–28.

Popov, P. P., and W. A. Sirignano. 2016. Transverse combustion instability in a rectangular rocket motor. *J. Propul. Power* 32:620–27. doi:10.2514/1.B35868.

Popov, P. P., W. A. Sirignano, and A. Sideris. 2015. Propellant injector influence on liquid-propellant rocket engine instability. *J. Propul. Power* 31:320–31. doi:10.2514/1.B35400.

Prieur, K., D. Durox, J. Beaunier, T. Schuller, and S. Candel. 2017a. Ignition dynamics in an annular combustor for liquid spray and premixed gaseous injection. *Proc. Combust. Inst.* 36:3717–24.

Prieur, K., D. Durox, J. Beaunier, T. Schuller, and S. Candel. 2017b. Ignition dynamics in an annular combustor for liquid spray and premixed gaseous injection. *Proc. Combust. Inst.* 36:3717–24.

Prieur, K., D. Durox, T. Schuller, and S. Candel. 2017b.A hysteresis phenomenon leading to spinning or standing azimuthal instabilities in an annular combustor. *Combust. Flame* 175:283–91. doi:10.1016/j.combustflame.2016.05.021.

Prieur, K., D. Durox, T. Schuller, and S. Candel. 2018. Strong azimuthal combustion instabilities in a spray annular chamber with intermittent partial blow-off. *J. Eng. Gas Turbines Power* 140:031503(10 pages). doi:10.1115/1.4037824.

Prieur, K., D. Durox, T. Schuller, and S. Candel. 2019. Flame and spray dynamics during the light round process in an annular system equipped with multiple swirl spray injectors. *J. Eng. Gas Turbines Power* 141:061007–11. doi:10.1115/1.4042024.

Putnam, A. A. 1971. *Combustion driven oscillations in industry*. New York: Elsevier.

Richecoeur, F., P. Scouflaire, S. Ducruix, and S. Candel. 2006. High-frequency transverse acoustic coupling in a multiple-injector cryogenic combustor. *J. Propul. Power* 22:790–99. doi:10.2514/1.18539.

Sattelmayer, T., and W. Polifke. 2003. Assessment of methods for the computation of linear stability of combustors. *Combust. Sci. Technol.* 175:453–76. doi:10.1080/00102200302382.

Schmid, P. J. 2010. Dynamic mode decomposition of numerical and experimental data. *J. Fluid Mech.* 656:5–28. doi:10.1017/S0022112010001217.

Schmitt, T., Y. Mery, M. Boileau, and S. Candel 2011. Large-Eddy Simulation of oxygen/methane flames under transcritical conditions. *Proc. Combust. Inst.* 33:1383–90.

Schuermans, B., F. Guethe, D. Pennell, D. Guyot, and C. O. Paschereit. 2010. Thermoacoustic modeling of a gas turbine using transfer functions measured under full engine pressure. *J. Eng. Gas Turbines Power* 132:111503(9 pages). doi:10.1115/1.4000854.

Schuermans, B., V. Bellucci, and C. Paschereit 2003. Thermoacoustic modeling and control of multiburner combustion systems. In ASME Conference Proceedings, Paper GT 2003-38688, ASME Turbo Expo, Atlanta, Georgia.

Schuller, T., D. Durox, and S. Candel. 2003. A unified model for the prediction of laminar flame transfer functions: Comparisons between conical and v-flames dynamics. *Combust. Flame* 134:21–34. doi:10.1016/S0010-2180(03)00042-7.

Silva, C., F. Nicoud, T. Schuller, D. Durox, and S. Candel. 2013. Combining a Helmholtz solver with the flame describing function to assess combustion instability in a premixed swirled combustor. *Combust. Flame* 160:1743–54. doi:10.1016/j.combustflame.2013.03.020.

Sirignano, W., and L. Crocco. 1964. A shock wave model of unstable rocket combustor. *Aiaa J.* 2:1285–96. doi:10.2514/3.2534.

Sirignano, W. A. 2015. Driving mechanisms for combustion instability. *Combust. Sci. Technol.* 187:162–205. doi:10.1080/00102202.2014.973801.

Sirignano, W. A., and J. Krieg. 2016. Two-time-variable perturbation theory for liquid-rocket combustion instability. *J. Propul. Power* 32:755–76. doi:10.2514/1.B35954.

Sirignano, W. A., and P. P. Popov. 2013. Two-dimensional model for liquid-rocket transverse combustion instability. *Aiaa J.* 51:2919–34. doi:10.2514/1.J052512.

Stow, S. R., and A. P. Dowling 2001. Thermoacoustic oscillations in an annular combustor. In ASME Conference Proceedings, Paper GT 2001-0037, ASME Turbo Expo, New-Orleans, Louisiana.

Thumuluru, S. K., and T. Lieuwen 2009. Characterization of acoustically forced swirl flame dynamics. *Proc. Combust. Inst.* 32:2893–900.

Töpperwien, K., T. Lancien, S. Puggelli, G. Vignat, K. Prieur. 2019. Large eddy simulation of flame dynamics during ignition of a swirling unit and comparison with experiments. In Proceedings of the 9th European Combustion Meeting, Lisbon, Portugal.

Tsien, H. S. 1952. The transfer functions of rocket nozzles. *J. Am. Rocket Soc.* 22:139–43. doi:10.2514/8.4448.

Urbano, A., L. Selle, G. Staffelbach, B. Cuenot, T. Schmitt, S. Ducruix, and S. Candel. 2016. Exploration of combustion instability triggering using large eddy simulation of a multiple injector liquid rocket engine. *Combust. Flame* 169:129–40. doi:10.1016/j.combustflame.2016.03.020.

Urbano, A., Q. Douasbin, L. Selle, G. Staffelbach, B. Cuenot, T. Schmitt, S. Ducruix, and D. Candel. 2017. Study of flame response to transverse acoustic modes from the LES of a 42-injector rocket engine. *Proc. Combust. Inst.* 36:2633–39. doi:10.1007/s10067-017-3885-1.

Vignat, G., D. Durox, A. Renaud, and S. Candel. 2020. High amplitude combustion instabilities in an annular combustor inducing pressure field deformation and flame blow-off. *J. Eng. Gas Turbines Power* 142:011016–1.

Vignat, G., D. Durox, K. Prieur, and S. Candel 2019. An experimental study into the effect of injector pressure loss on self-sustained combustion instabilities in a swirled spray burner. *Proc. Combust. Inst.* 37:5205–13.

Worth, N., and J. Dawson. 2019. Characterisation of flame surface annihilation events in self excited interacting flames. *Combust. Flame* 199:338–51. doi:10.1016/j.combustflame.2018.10.032.

Worth, N. A., and J. R. Dawson. 2013a. Modal dynamics of self-excited azimuthal instabilities in an annular combustion chamber. *Combust. Flame* 160:2476–89. doi:10.1016/j.combustflame.2013.04.031.

Worth, N. A., and J. R. Dawson 2013b b. Self-excited circumferential instabilities in a model annular gas turbine combustor: Global flame dynamics. *Proc. Combust. Inst.* 34:3127–34.

Worth, N. A., J. R. Dawson, J. A. M. Sidey, and E. Mastorakos 2017. Azimuthally forced flames in an annular combustor. *Proc. Combust. Inst.* 36:3783–90.

Xia, Y., C. Linghu, Y. Zheng, C. Ye, C. Ma, H. Ge, and G. Wang. 2019. Experimental investigation of the flame front propagation characteristic during light-round ignition in an annular combustor. *Flow Turbul. Combust.* 103:247–69. doi:10.1007/s10494-019-00018-y.

Yang, D., A. Laera, and A. Morgans. 2019. A systematic study of nonlinear coupling of thermoacoustic modes in annular combustors. *J. Sound Vib.* 456:137–61. doi:10.1016/j.jsv.2019.04.025.

Zinn, B., and L. Crocco. 1968. Nozzle boundary condition in nonlinear rocket instability problem. *Astronaut. Acta* 13:489.